

Mutual Diffusivities of Mixtures of Carbon Dioxide and Hydrogen and Their Solubilities in Brine: Insight from Molecular Simulations

Thejas Hulikal Chakrapani, Hadi Hajibeygi, Othonas A. Moulton, and Thijs J. H. Vlugt*



Cite This: *Ind. Eng. Chem. Res.* 2024, 63, 10456–10481



Read Online

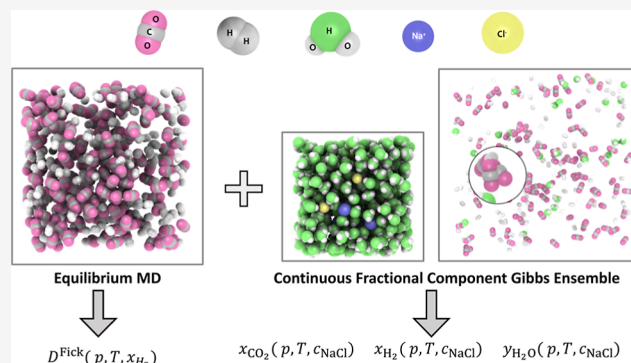
ACCESS |

Metrics & More

Article Recommendations

Supporting Information

ABSTRACT: $\text{H}_2\text{-CO}_2$ mixtures find wide-ranging applications, including their growing significance as synthetic fuels in the transportation industry, relevance in capture technologies for carbon capture and storage, occurrence in subsurface storage of hydrogen, and hydrogenation of carbon dioxide to form hydrocarbons and alcohols. Here, we focus on the thermodynamic properties of $\text{H}_2\text{-CO}_2$ mixtures pertinent to underground hydrogen storage in depleted gas reservoirs. Molecular dynamics simulations are used to compute mutual (Fick) diffusivities for a wide range of pressures (5 to 50 MPa), temperatures (323.15 to 423.15 K), and mixture compositions (hydrogen mole fraction from 0 to 1). At 5 MPa, the computed mutual diffusivities agree within 5% with the kinetic theory of Chapman and Enskog at 423.15 K, albeit exhibiting deviations of up to 25% between 323.15 and 373.15 K. Even at 50 MPa, kinetic theory predictions match computed diffusivities within 15% for mixtures comprising over 80% H_2 due to the ideal-gas-like behavior. In mixtures with higher concentrations of CO_2 , the Moggridge correlation emerges as a dependable substitute for the kinetic theory. Specifically, when the CO_2 content reaches 50%, the Moggridge correlation achieves predictions within 10% of the computed Fick diffusivities. Phase equilibria of ternary mixtures involving $\text{CO}_2\text{-H}_2\text{-NaCl}$ were explored using Gibbs Ensemble (GE) simulations with the Continuous Fractional Component Monte Carlo (CFCMC) technique. The computed solubilities of CO_2 and H_2 in NaCl brine increased with the fugacity of the respective component but decreased with NaCl concentration (salting out effect). While the solubility of CO_2 in NaCl brine decreased in the ternary system compared to the binary $\text{CO}_2\text{-NaCl}$ brine system, the solubility of H_2 in NaCl brine increased less in the ternary system compared to the binary $\text{H}_2\text{-NaCl}$ brine system. The cooperative effect of $\text{H}_2\text{-CO}_2$ enhances the H_2 solubility while suppressing the CO_2 solubility. The water content in the gas phase was found to be intermediate between $\text{H}_2\text{-NaCl}$ brine and $\text{CO}_2\text{-NaCl}$ brine systems. Our findings have implications for hydrogen storage and chemical technologies dealing with $\text{CO}_2\text{-H}_2$ mixtures, particularly where experimental data are lacking, emphasizing the need for reliable thermodynamic data on $\text{H}_2\text{-CO}_2$ mixtures.



1. INTRODUCTION

The need to meet growing global energy demands while controlling carbon emissions has brought underground hydrogen storage to the forefront.^{1–4} Given the intermittent production of renewable energy sources such as wind and solar, storing excess energy becomes essential to ensure consistent supply.⁵ Converting surplus energy into hydrogen by water electrolysis is a desirable method, given the appeal of hydrogen as an energy carrier: low carbon footprint and high mass-specific energy density.^{1–4} At present, worldwide hydrogen consumption stands at approximately 115 million metric tons (115×10^9 kg) per year³ and is expected to increase 10-fold (to the gigatonnes per year scale) to accommodate the expanding global energy needs.³ Storing a gigatonne of hydrogen would necessitate immense storage volumes of the order of 10^{11} m^3 , even at significant pressures of 10 MPa and temperatures of 323.15 K.³ Only geological formations such as depleted gas reservoirs and salt caverns can offer such large

volumes for hydrogen storage.³ Depleted gas reservoirs, used initially for natural gas storage, can also be used for hydrogen storage.^{1–3,6} A so-called cushion gas is injected into a gas reservoir to maintain its pressure,^{2,3} while brine (or salt water) is naturally present within the reservoir.^{2,3} Processes such as the mixing of hydrogen with the cushion gas via molecular diffusion, and its dissolution into brine can decrease the purity of the stored hydrogen.^{1,3,6} Thus, estimating the mutual diffusion coefficients characterizing gas mixing and the solubility of the resulting gas mixtures in brine is essential

Received: March 21, 2024

Revised: May 14, 2024

Accepted: May 20, 2024

Published: May 31, 2024



ACS Publications

for enabling underground storage of hydrogen.^{2,3} Oldenburg and colleagues^{7,8} showed that using carbon dioxide (CO_2) as a cushion gas facilitates efficient injection and production of natural gas due to its high compressibility at reservoir-relevant thermodynamic conditions. CO_2 is opted as the cushion gas in our study due to the similarities between hydrogen and natural gas storage.⁴

1.1. Fick Diffusivities of $\text{CO}_2\text{-H}_2$ Mixtures. Mass transport in binary gas mixtures, in the absence of temperature and pressure gradients, is described by Fick's law, which linearly relates the diffusive flux to the concentration gradient of a species.^{9–11} An alternative description of the same phenomenon can be formulated by the Maxwell–Stefan (MS) framework,¹² which describes diffusive mass transport based on chemical-potential gradients. The proportionality constant in Fick's law, denoted by the mutual or Fick diffusion coefficient,^{10,11} can exhibit a strong dependence on the temperature, pressure, and mixture composition.^{10,11} Analytic expressions, experimental measurements, semiempirical methods guided by theory, and numerical simulations have been used to calculate mutual diffusivities in binary gas mixtures.^{11,13–15} Chapman and Enskog^{16–18} independently derived an analytic expression to predict the mutual diffusion coefficients of binary gas mixtures by solving the Boltzmann transport equation in the dilute gas limit in a framework commonly referred to as the kinetic theory of gases.^{14,16–18} Kinetic theory assumes gases are made of monatomic, spherical, nonpolar particles that undergo elastic collisions, i.e., there are no strong molecular interactions between them. The prediction of diffusivities by Chapman and Enskog has been shown to be highly accurate in the dilute gas regime.^{19–21} At moderate to high pressures (less than tens of MPa¹¹), the applicability of kinetic theory for dilute gases is in doubt due to its simplistic assumptions of intermolecular interactions.^{11,17,18} Many researchers have expanded kinetic theory to address scenarios involving dense gases,^{14,17,22} notably the work of van Beijeren and Ernst, who derived diffusion coefficients and other properties for moderately dense, multicomponent mixtures of hard spheres, known as the revised Enskog theory (RET).²² Jervell and Wilhelmsen²³ recently presented an RET for multicomponent mixtures of Mie fluids (RET-Mie), which is claimed to accurately predict transport properties such as diffusion coefficients, thermal diffusivities, viscosities, and thermal conductivities. With parameters of the Mie-potentials fitted to equilibrium properties of the respective components, predictions of mutual diffusivities of noble gases for pressures ca. 0.1 MPa for a wide temperature range (200–1400 K) are within 4% of the experimental data.^{24,25} RET-Mie predictions of self-diffusivities of H_2 are within 10% of the available experimental data up to 200 MPa and at temperatures between 171 and 372 K, and mutual diffusivities of noble gases are predicted within 4% of the experimentally determined values. Fick diffusivities of carbon dioxide-methane (CH_4) mixtures are within 20% of experimental measurements and molecular simulations for pressures up to 14.7 MPa.²⁶ Except for xenon in the vicinity of the critical point, the thermal conductivity of noble gases and their mixtures is reproduced within 10% of the experimental data at 300 K and pressures between 0.01 and 10 MPa. RET-Mie predictions of the viscosity are within ca. 10% of the experimental data for methane, nitrogen, and argon up to 300 bar for temperatures ranging between 233 and 523 K. At pressures up to 500 bar and temperatures from 200 to 800 K, the predictions are within ca. 15% of the most accurate

correlation for the viscosity of air. Larger inaccuracies in the predictions of mutual diffusivities of $\text{CO}_2\text{-CH}_4$ mixtures reflect the inability of the theory to account for nonspherical shapes of molecules. In conclusion, kinetic theory is incapable of predicting the mutual diffusivities of $\text{CO}_2\text{-H}_2$ mixtures at reservoir-relevant thermodynamic conditions due to its simplistic assumptions. Advanced theories such as the RET-Mie (or RET) are cumbersome to use and still require significant efforts to account for nonspherical molecules.^{14,23}

Marrero and Mason¹⁹ and Li et al.²⁷ provide an extensive review of experimental data on the mutual diffusivities in binary mixtures of CO_2 and H_2 , a summary of which can be found in Table 1. This table highlights the extensive literature containing data for a wide range of temperatures, albeit confined to pressures near the atmospheric pressure (0.1

Table 1. List of Experimental Studies Reporting Diffusion Coefficients of Binary Mixtures of Hydrogen and Carbon Dioxide^a

study	temperature/[K]	experimental method ^{11,19}
Loschmidt ¹⁴¹	273 and 286	closed tube
Loschmidt ¹⁴²	273–289	closed tube
Schmidt ¹⁴³	288	closed tube
Lonius ¹⁴⁴	286–294	closed tube
Boardman and Wild ¹⁴⁵	288	closed tube
Suetin ¹⁴⁶	273	closed tube
Wrestschko	297	closed tube
Suetin and Ivakin ¹⁴⁷	292	closed tube
Ivakin and Suetin ¹⁴⁸	292–473	closed tube
von Obermayer ¹⁴⁹	285–335	open tube
von Obermayer ¹⁵⁰	284–293	open tube
von Obermayer ¹⁵¹	280–294	open tube
Schäfer et al. ¹⁵²	252–308	two-bulb
Lonsdale and Mason ¹⁵³	259–358	two bulb
Saxena and Mason ¹³⁶	250–368	two bulb
Bondarenko and Golubev ¹⁵⁴	323–363	two bulb
Miller and Carman ¹⁵⁵	293	two bulb
Annis et al. ¹⁵⁶	295	two bulb
Miller and Carman ¹⁵⁷	293	two bulb
Waldmann ^{158,159}	293	Dufour effect
Mason et al. ¹⁶⁰	296	Dufour effect
Weissman ¹³⁷	298–500	from mixture viscosities
Kestin et al. ¹⁶¹	295.15, 300.65 and 303.15	from mixture viscosities
Wicke and Hugo ¹⁶²	295	diffusion bridge
Schneider and Schäfer ¹⁶³	273–990	diffusion bridge
Kosov and Zhalgasov ¹⁶⁴	196–298	diffusion bridge
Giddings and Seager ¹⁶⁵	300	gas chromatography
Gavril et al. ¹³⁵	315.2–343.9	reverse liquid gas chromatography
Boyd et al. ¹⁶⁸	298	thermal separation
Vyshenskaya and Kosov ¹⁶⁶	293–1083	capillary leak
McCarty and Mason ¹⁶⁷	303	Kirkendall effect

^aThe pressures in the various studies are all close to atmospheric pressure. A detailed discussion of the experimental methods can be found in the article by Marrero and Mason¹⁹ and the textbook by Cussler¹¹ and in references therein.

MPa). Chou and Martin²⁸ measured the self-diffusion coefficients of infinitely diluted Carbon-14 labeled C¹⁴O₂ in ternary mixtures of C¹⁴O₂, CO₂, and H₂ for temperatures of 308.15 and 373.15 K, and pressures of 0.6 and 25.33 MPa. Literature covering experimental studies of trace solutes in dense gases, such as supercritical CO₂, has been summarized by Poling et al.¹³ To the best of our knowledge, experimental data for the Fick diffusivities of binary mixtures of CO₂ and H₂ at pressures exceeding the atmospheric pressure have not been reported.

To facilitate rapid and precise predictions of Fick diffusivities in gas mixtures, numerous semiempirical expressions guided by the kinetic theory have been developed.^{11,13} These expressions aim to fill the gap resulting from the scarcity of experimental measurements, specifically for predicting binary diffusion coefficients in both dilute and dense gases.¹³ Correlations by Wilke-Lee²⁹ and Fuller et al.^{30–32} are often used to predict diffusion coefficients in dilute gas mixtures. These correlations fail at high pressures,^{11,13} just as Chapman and Enskog's analytic expression for mutual diffusivities, and cannot take into account the compositional dependence of the mixture. Several methods have been proposed to estimate diffusion coefficients in dense gas mixtures.¹³ Takahashi and Hongo³³ and Riazi and Whitson³⁴ suggested empirical equations based on the method of corresponding states to correlate the product of pressure and diffusion coefficient at low and high pressures.¹³ Takahashi and Hongo's correlation for the effect of pressure and temperature on the binary diffusion coefficient requires the evaluation of an empirical equation using look-up tables that are tabulated as functions of the critical temperature and pressure of the components in the mixture.¹³ Riazi and Whitson's correlation requires the viscosity of the mixture as an input and does not yield the correct value of mutual diffusivities in the limit of low pressure.¹³ No correlation is entirely satisfactory for predicting mutual diffusivities at both low and high pressures, primarily due to the simplistic assumptions of the theory of corresponding states.¹³ Although semiempirical methods are relatively easy to use and computationally fast, their accuracy depends on the extent and quality of the experimental data that was used for their development. Generally, one needs to exercise caution when using semiempirical methods outside the range used for its calibration.

Predictions of Fick diffusivities for binary mixtures of CO₂-H₂ using semiempirical methods can be accurate between low to intermediate pressures but can be inaccurate due to neglecting strong molecular interactions emanating at large pressures (\gtrsim 10 MPa). Molecular dynamics (MD) simulations, a potent tool in materials research,^{35,36} operate at atomistic length and time scales, offering insights at the molecular-scale.^{35,36} The formulation of accurate force fields for multiple components, the design of efficient algorithms, coupled with advancements in computational power, has made MD a go-to method for calculating the diffusivities of pure components, mixtures, and other transport properties of fluids.^{35,36} The data obtained from MD simulations has been used for the development of engineering models and the validation of semiempirical approaches.^{37–39} Mutual diffusivities in binary and ternary fluid mixtures have been computed using MD simulations and have been successfully validated with experimental data.^{40–42} In sharp contrast, the Fick diffusivities of binary gas mixtures computed from MD simulations have not received much attention. Vella⁴³ computed Fick

diffusivities for CO₂-CH₄ mixtures using MD simulations at temperatures and pressures corresponding to the dilute and dense regimes. The computed diffusivities (within statistical uncertainties), described faithfully by Fuller's correlation,^{30–32} agreed with the experimental data between 293 and 500 K and 1.01325 MPa (dilute gas regime). Deviations exceeding 40% were observed between Fuller's correlation and the computed diffusivities at ca. 310 K and pressures above ca. 2 MPa (the dense gas regime). Due to the lack of experimental data in the dense gas regime, Vella⁴³ was unable to confirm the accuracy of the Fick diffusivities computed by MD simulations. Guevara-Carrion²⁶ compared the measured Fick diffusivities of very dilute CH₄ in supercritical CO₂ at temperatures of 292.55 and 332.85 K and pressures of 9, 12.5, and 14.7 MPa. The mutual diffusivities changed from liquid-like to gas-like values within a small temperature range near the supercritical region across the so-called Widom line.²⁶ Saric et al.⁴⁴ measured the mutual diffusivities of binary mixtures of H₂ diluted in CO₂, along with other binary gas mixtures. Three mole fractions of H₂, representing the infinite-dilution limit (mostly 0.5, 1.0, and 1.5 mol %), were examined between 290 and 350 K at 9 MPa. Saric et al.⁴⁴ proposed a simple equation to predict the Widom line of dilute supercritical CO₂ mixtures as a function of pressure, solute mole fraction, and critical properties of the mixture components. In a separate study, Saric et al.⁴⁵ examined the mutual diffusion of various hydrocarbons dispersed in supercritical carbon dioxide via MD simulations near the Widom line, between 290 and 345 K at 9 MPa. Fick diffusivities were strongly affected close to the critical region of the mixture due to the pronounced clustering of solute molecules. Saric et al.⁴⁵ pointed out that the validity of the Stokes-Einstein relation near the Widom line was questionable. A correlation function was proposed to facilitate quick calculations of Fick diffusivities for various binary mixtures.

Rosenfeld⁴⁶ proposed an empirical correlation connecting transport properties to the excess entropy of a fluid at a given temperature and pressure. This semiquantitative model has garnered renewed interest since the early 2000s,^{47–50} demonstrating its broader applicability beyond simple liquids.^{49–51} Despite its nonrigorous nature, the concept of excess entropy could serve as a valuable tool in connecting thermodynamics and dynamics for predicting transport properties in mixtures.^{47,48}

To summarize, neither experimental data nor MD simulations have reported the Fick diffusivities of CO₂-H₂ mixtures under reservoir conditions. Analytic expressions can be cumbersome and require effort to include nonspherical molecules.^{14,17,23} Semiempirical methods, though easy to use, are not accurate for the entire range of thermodynamic conditions of interest.^{11,13}

1.2. Vapor-Liquid Equilibria for Systems Involving H₂, CO₂, and NaCl Brine. **1.2.1. CO₂-NaCl Brine Systems.** Understanding the dissolution of H₂ in saline water, referred to as brine, at various thermodynamic conditions is necessary for estimating hydrogen purity during subsurface storage. This involves predicting solubilities by assessing equilibrium between vapor and liquid phases in a multicomponent system at different temperatures and pressures, known as vapor-liquid equilibria (VLE).^{13,52,53} VLE of CO₂-NaCl brine (or H₂-NaCl brine) is determined via experiments, equation-of-state models, and force field-based molecular simulations.^{54–67}

Studies by Spycher et al.^{54,55} and Mutailipu provide an overview of the VLE of various CO₂-brine systems compiled from experimental studies. Spycher et al.⁵⁴ compared data on mutual solubilities in CO₂-H₂O mixtures from various experiments for pressures up to 50 MPa and temperatures below 373.15 K. Solubilities measured in the two-phase region, where a CO₂-rich phase (usually gas) coexists with a H₂O-rich liquid phase, were consistent across various studies.⁵⁴ A thermodynamic model was developed by Spycher et al.⁵⁴ based on the Redlich-Kwong equation-of-state to enable quick predictions of mutual solubilities in CO₂-H₂O systems. This model predicts mutual solubilities with an accuracy of a few percent of the experimental data for pressures up to 60 MPa and a temperature ca. 383.15 K. In a subsequent study, Spycher et al.⁵⁵ extended the thermodynamic model developed initially for CO₂-H₂O mixtures⁵⁴ to include the influence of chloride salts dissolved in the aqueous phase. The extended thermodynamic model to predict mutual solubilities included activity coefficients for aqueous CO₂ derived from studies developed primarily for sodium chloride (NaCl). The activity coefficients of NaCl provided by Duan and Sun⁵⁶ and Rumpf et al.⁶⁸ were shown to yield CO₂ solubilities in NaCl brine that were closest to the experiments by Duan and Sun,⁵⁶ Drummond,⁶⁹ Malinin and Saveleva,⁷⁰ Malinin and Kurkovskaya,⁷¹ Rumpf et al.,⁶⁸ Nighswander et al.,⁷² Bando et al.,⁷³ and Kiepe et al.,⁷⁴ between pressures 3.5 and 6.8 MPa and between 293.15 K and 373.15 K. The extended solubility model provided by Spycher and Pruess,⁵⁵ including the effect of salts, was shown to be accurate to within the experimental uncertainty for solutions up to 6 molal (= moles of salt per kg of water) for NaCl and 4 molal for CaCl₂. Spycher and Pruess⁷⁵ extended their solubility model⁵⁵ to cover temperatures up to 573 K (from 285 K) and pressures below 60 MPa.

Molecular simulations have been extensively applied to investigate VLE in CO₂-H₂O and CO₂-NaCl brine systems. Vorholz et al.⁶³ studied the VLE of H₂O between 323 and 573 K, CO₂ between 230 and 290 K, and CO₂-H₂O mixtures between 348 and 393 K using NVT and NPT versions of Gibbs Ensemble Monte Carlo^{35,36} (GEMC) simulations. Three different H₂O force fields, namely SPC, SPC-E, and TIP4P, the EPM2 force field for CO₂, and combinations thereof were examined to find the optimal VLE description for binary mixtures of CO₂-H₂O. The best prediction for the VLE of CO₂-H₂O binary mixtures, up to pressures of 20 MPa, was achieved by combining the SPC and TIP4P force fields for water with the EPM2 force field for carbon dioxide. Liu et al.⁶⁰ used histogram-reweighting Grand-Canonical Monte Carlo (GCMC)^{35,36} simulations to obtain the phase behavior of CO₂-H₂O mixtures for 323.15 and 723.15 K, and 0 and 100 MPa. Several different force fields for H₂O and CO₂ were tested using the conventional Lorentz-Berthelot mixing rules^{35,36} for the interaction between unlike atoms. Experimentally measured solubilities deviated from solubilities computed using force field based simulations for the entire range of temperatures and pressures spanning 323.15 to 723.15 K and 0 to 100 MPa, respectively. The work of Liu et al.⁶¹ suggests the need for improved atomistic force fields to accurately predict the VLE of CO₂-H₂O systems. Liu et al.⁶¹ investigated the phase behavior and interfacial tension of CO₂-H₂O-NaCl mixtures using MD simulations between 323.15 and 523.15 K, 0–60 MPa, and NaCl concentrations 1–4 molal. TraPPE^{76,77}/TIP4P2005⁷⁸ performed the most effectively among various combinations of force fields evaluated for

predicting the VLE of the H₂O-CO₂-NaCl system. The dependence of the interfacial tension on temperature, pressure, and salt concentration was also examined, revealing insights into the predictive capabilities of different force field combinations. Orozco et al.⁶² conducted NPT GEMC simulations to obtain optimized intermolecular potential parameters to describe the phase behavior of CO₂-H₂O mixtures. The simulations covered a temperature range of 423–523 K and pressures from 20 to 80 MPa, addressing conditions pertinent to carbon capture and sequestration processes. Lobanova et al.⁶⁴ simulated the VLE for CO₂-H₂O systems at 423 and 548 K using the SAFT-CG Mie force-fields for CO₂ and H₂O. The solubilities agreed well with various experimental data sources, thus allowing for an accurate description of CO₂-H₂O mixtures. Using GEMC simulations, Jiang et al.⁶⁵ explored the phase equilibria of H₂O/CO₂ and H₂O/n-alkane mixtures between 323 and 523 K and 20 and 80 MPa. CO₂ solubility in water was computed for combinations of three polarizable models for water and a polarizable Gaussian charge model for CO₂. Accurate compositions for both H₂O and CO₂-rich phases were achieved using hydrogen bonding parameters derived from the second virial coefficient for H₂O-CO₂ mixtures.

1.2.2. H₂-NaCl Brine Systems. A summary of H₂ solubilities in pure H₂O and brine can be found in the works by Chabab et al.,^{57,59} Ansari,⁵⁸ and Torín-Ollarves and Trusler.⁷⁹ Recognizing the lack of data for pressures exceeding 0.1 MPa, Chabab et al.⁵⁷ conducted experiments to measure the solubility of H₂ in brine, specifically NaCl brine, with molality ranging from 0 to 6 molal. Experiments were conducted between 323 and 373 K and 0.1–23 MPa. To enable quick and accurate predictions of H₂ solubilities in brine as functions of temperature, pressure, and molality, the e-PR-CPA⁸⁰ (electrolyte-Peng-Robinson⁸¹-Cubic Plus Association^{82–84}) model was used, which was parametrized using the H₂ solubilities from experiments. Torín-Ollarves and Trusler⁷⁹ reported H₂ solubilities in NaCl brine at a salt concentration of 2.5 molal between 323.15 and 423.15 K, up to pressures of 40 MPa. Following Krichevsky and Kasarnovsky,⁸⁵ Torín-Ollarves and Trusler⁷⁹ developed a correlation describing the solubility of H₂ in H₂O and NaCl brines for temperatures between 273.15 and 423.15 K and for pressures up to 100 MPa. Although the solubilities of H₂ in salt-free water, as reported by Chabab et al.,⁵⁷ conformed with the thermodynamic model proposed by Torín-Ollarves and Trusler,⁷⁹ the solubilities of H₂ in NaCl brine (up to 5 molal) were underestimated by approximately 25% when compared to an extended Krichevsky-Kasarnovsky model.⁸⁵ This discrepancy was observed at temperatures of 323.2 and 372.7 K, considering H₂ partial pressures up to 20 MPa. In a recent study, Chabab et al.⁵⁹ addressed inconsistencies in H₂ solubilities in NaCl brine for different experimental sources. These authors contributed new solubility data for H₂ in NaCl brine, covering the temperature range of 298 to 373 K, with a NaCl concentration of 4 molal and pressures up to 20 MPa. The H₂ solubilities measured in the work by Chabab⁵⁹ are between those measured in an earlier study by Chabab et al.⁵⁷ and Torín-Ollarves and Trusler.⁷⁹ The H₂ solubility data were used to parametrize and assess three different thermodynamic models: (1) the e-NRTL activity coefficient model,^{86,87} (2) the Duan-type (noniterative) model,^{88,89} and (3) the Søreide and Whitson's equation of state.⁹⁰ These models were shown to be highly accurate in predicting the phase equilibria of H₂-NaCl

brine systems, with an average absolute deviation of less than 3%.⁵⁹

H_2 solubilities in H_2O and NaCl brine have also been studied using molecular simulations.^{66,91} Rahbari et al.⁶⁶ reported H_2 solubilities in H_2O calculated from Monte Carlo simulations for pressures between 1 and 100 MPa and temperatures between 283 and 423 K. The H_2 solubilities calculated using molecular simulations were in excellent agreement with the experimental data at high pressures by Wiebe and Gaddy.⁹² In another article, Rahbari et al.⁹³ studied the VLE of hydrogen-water mixtures along the melting line of ice Ih, corresponding to temperatures between 264.21 and 272.4 K. Based on the computed solubility data of H_2 in H_2O , the freezing point depression of water caused by NaCl was calculated for temperatures between 264.21 and 272.4 K. Lopez-Lazaro et al.⁹⁴ computed the solubilities of H_2 in aqueous NaCl solutions using molecular simulations for molalities up to a maximum of 2 molal between temperatures of 280 and 350 K. Recently, van Rooijen et al.⁹⁵ reported H_2 solubilities in aqueous NaCl solutions for temperatures between 298 and 363 K, pressures ranging between 0.1 and 100 MPa, and molalities between 0 and 6 molal, together with other thermodynamic properties such as interfacial tensions and transport properties of H_2 - H_2O -NaCl systems. The H_2 concentrations in NaCl brine, calculated using molecular simulations,⁹⁵ are larger compared to the predictions by Chabab et al.⁵⁷ and lower than the prediction by Torín-Ollarves and Trusler⁷⁹ for NaCl molalities larger than 0.5 molal. Despite numerous studies exploring solubilities in CO_2 -NaCl brine and H_2 -NaCl brine systems for diverse temperatures and pressures, there is a lack of data regarding solubilities in CO_2 - H_2 -NaCl brine systems.

Recognizing the lack of information on binary Fick diffusivities in CO_2 - H_2 mixtures at high pressures, temperatures, and various compositions and the limited understanding of the VLE in ternary systems of CO_2 - H_2 -NaCl brine, molecular simulations are performed to address this gap. This study investigates the Fick diffusion coefficients computed from equilibrium MD simulations of H_2 - CO_2 mixtures. Driven by the thermodynamic conditions relevant to subsurface hydrogen storage, simulations are performed covering temperatures between 323.15 and 423.15 K, 5–50 MPa, and mole fractions of hydrogen (x_{H_2}) varying from 0 to 1. Solubilities of H_2 - CO_2 mixtures in pure water and NaCl brine at concentrations of 1 and 2 mol of NaCl per kg water are calculated using the isothermal-isobaric version of the Continuous Fractional Component Gibbs Ensemble (CFCGE) Monte Carlo technique.^{96–100} Temperatures between 323.15 and 423.15 K and pressures between 5 and 50 MPa are explored. We only examine ternary mixtures where the overall mole fractions of CO_2 , H_2 , and Brine, calculated using the total number of molecules in both the gas and liquid phases, are 1/6, 1/6, and 2/3, respectively.

This paper is organized as follows: Section 2 provides details on the force fields and molecular simulation techniques. In Section 3, the self-diffusivities of H_2 and CO_2 are compared, along with the mutual diffusivities and solubilities obtained via molecular simulations. Comparisons to available experimental data and analytic expressions are included. Concluding remarks are presented in Section 4. All computed raw data from this study are tabulated in the Supporting Information.

2. METHODS

2.1. Force Fields. The TraPPE force field is used to simulate CO_2 as a rigid linear molecule.^{76,77} TraPPE compares favorably with experimental data for the VLE of pure CO_2 and its multicomponent mixtures for a wide range of temperatures, pressures, and compositions.^{76,77} The three-site Marx force field^{101,102} is used to simulate H_2 as a rigid body for its accuracy in reproducing the bulk densities and fugacities of H_2 at pressures up to 100 MPa.^{66,103} Quantum effects emanating at low temperatures are insignificant for the temperatures considered in this work (323.15–423.15 K).^{104,105} Water is simulated as a rigid body using the TIP4P/ μ force field, a modified version of the TIP4P/2005 model⁷⁸ developed by Rahbari and colleagues.⁶⁶ The TIP4P/ μ force field accurately predicts the VLE of H_2O - H_2 mixtures between 323 and 423 K and 10–100 MPa⁶⁶ as it was partially trained to reproduce the excess chemical potential of liquid water. The Madrid-2019 force field¹⁰⁶ is used to model the Na^+ and Cl^- ions, which are parametrized for the TIP4P/2005 H_2O force field.⁷⁸ Lennard-Jones (LJ) and electrostatic interactions are calculated for all species. All interaction parameters used in this study are listed in Table S1 of the Supporting Information. The Lorentz–Berthelot (LB) mixing rules^{35,36} are applied in most cases barring a few exceptions, see Table S1 of the Supporting Information.

2.2. Molecular Dynamics. MD simulations were performed using the Large-scale Atomic/Molecular Massively Parallel Simulator (LAMMPS)¹⁰⁷ (version 23 June 2022) to calculate the self- and Fick diffusivities in CO_2 - H_2 mixtures. Pressures between 5 and 50 MPa in 5 MPa increments, temperatures between 323.15 and 423.15 K in 25 K increments, and hydrogen mole fractions between 0 and 1 in 0.1 increments were explored. At these thermodynamic conditions, H_2 - CO_2 mixtures exhibit either gas- or dense-gas-like behavior.¹⁰⁸ Simulation boxes are periodic in all three directions. Equations of motion are integrated using the velocity-Verlet algorithm using a time step of 0.5 fs. Lennard-Jones and long-range electrostatic molecular interactions are calculated with a cutoff radius of 10 Å, supplemented by tail corrections for energy and pressure. All long-range electrostatic interactions are computed using the Particle–Particle Particle-Mesh method with a relative precision of 10^{-6} . Neighbor lists for every molecule are generated each time step using a binning procedure by considering a radius equal to the force cutoff of 10 Å plus an additional “skin” of thickness 3 Å.

Transport properties such as viscosities, self-, MS, and Fick diffusivities are computed in the NVE ensemble using systems of 120 molecules. Small systems of 120 molecules are chosen to manage the high computational demands associated with the gas phase simulations for the calculation of (self- and MS) diffusivities for trajectories typically lasting 100 ns. Accurate computation of transport properties requires correction for finite-size effects, a topic addressed in Section 2.2.1. To ensure that simulations in the NVE ensemble yield the correct average pressure and temperature, the box sizes and total system energy (in $kJ\cdot mol^{-1}$) are determined from independent simulations of 2000 molecules. Small systems of 120 molecules are unsuitable for computations of densities due to the possibility of the interaction cutoff radii exceeding half of the box size, violating the nearest image convention. Long simulations in the NVT phase are necessary to obtain an average temperature due to the substantial fluctuations

resulting from the small system size. The procedure and the raw data of the simulations for the larger systems are described and tabulated in [Section S1.1](#) and [Table S2](#) of the Supporting Information.

2.2.1. Calculation of Transport Properties. Viscosities describe momentum transport,¹⁰⁹ while self-, MS, and Fick diffusivities elucidate mass transport.^{10,109,110} Self-diffusion of a molecule in a fluid is caused by Brownian motion and occurs irrespective of gradients in chemical potential, temperature, or pressure.¹¹⁰ In contrast, MS and Fick diffusion^{10,109} describe the collective motion of molecules in response to gradients in chemical potential and concentration, respectively. Self-, MS, and Fick diffusion all contribute to mass transport via random or directed molecular motion, as explained in various texts.^{10,109,110} Viscosities, self-, MS, and Fick diffusivities are calculated in the *NVE* ensemble. The simulation box size corresponds to the density determined from systems of 2000 molecules, and the (scaled) total energy is imposed to obtain the desired temperature. Simulations consist of an initialization phase lasting 1 ns to achieve equilibration, followed by a production phase lasting between ca. 30–150 ns. The duration of the production phase varies widely due to density variations, affecting computational demands. Simulations at higher densities (e.g., systems at 50 MPa and 323.15 K) are computationally cheaper than those at lower densities (e.g., systems at 5 MPa and 423.15 K). During the production phase, the OCTP plugin¹¹¹ in LAMMPS¹⁰⁷ is used to compute the shear viscosities and self- and MS diffusivities based on mean-squared displacements. A discussion of the equations and methods to compute transport properties in the OCTP plugin can be found in the article by Jamali et al.¹¹¹ Calculation of Fick diffusivities from MS diffusivities requires the so-called thermodynamic factors of diffusion.^{10,11,40–42,112,113} Recently, Vlugt and co-workers¹¹⁴ showed that the thermodynamic factors (Γ) computed using the CFCMC technique^{96–100,115} for various CO₂-H₂ mixtures at 323.15 K and pressures of 5 and 50 MPa agreed within 3% of the REFPROP data.¹⁰⁸ Thus, for convenience and efficiency, thermodynamic factors for H₂-CO₂ mixtures are computed by numerically differentiating the Margules activity coefficient model based on the excess Gibbs energies obtained from REFPROP,¹⁰⁸ as discussed in [Section S5](#). To obtain accurate values of transport properties, an average value is calculated over 5 independent simulations at each thermodynamic state point. Uncertainties in the computed transport properties are calculated as the standard deviation across these 5 independent simulations.

While viscosities are usually unaffected by finite-size effects,^{116,117} self-, MS, and Fick diffusivities can depend on the system size,^{116,118,119} particularly in dense systems.¹¹⁷ The finite-size correction to the self-diffusion coefficient proposed by Yeh and Hummer^{118,120} is

$$D_i^{\text{self}} = D_i^{\text{self,MD}} + D^{\text{YH}}(T, \eta, L) = D_i^{\text{self,MD}} + \frac{k_B T \xi}{6\pi\eta L} \quad (1)$$

where D_i^{self} is the finite-size corrected self-diffusivity of the i th species, ξ is a dimensionless constant equal to 2.837298, and L is the box length of a cubic simulation box. Jamali et al.¹¹⁶ showed that the MS diffusion coefficients can be corrected according to

$$D^{\text{MS}} = D^{\text{MS,MD}} + \frac{D^{\text{YH}}}{\Gamma} \quad (2)$$

where D^{MS} is the finite-size corrected MS diffusivity, D^{YH} is the Yeh–Hummer correction term in [eq 1](#),¹¹⁸ and Γ is the thermodynamic factor for diffusion. For ideal mixtures where cross-correlations between molecular displacements of different species are negligible, the MS diffusivities follow the Darken equation^{11,116,121,122}

$$D^{\text{MS}} \approx D^{\text{Darken}} = x_2 D_1^{\text{self}} + x_1 D_2^{\text{self}} \quad (3)$$

Taking advantage of the relation between D^{MS} and D^{Fick} ,¹² Jamali et al.¹¹⁶ showed that the correction for the Fick diffusivity follows^{116,118}

$$D^{\text{Fick}} = \Gamma D^{\text{MS}} = D^{\text{Fick,MD}} + D^{\text{YH}} \quad (4)$$

2.3. Monte Carlo Simulations. VLEs of CO₂-NaCl brine mixtures, H₂-NaCl brine mixtures, and CO₂-H₂-NaCl brine mixtures are determined via MC simulations performed using the open-source Brick-CFCMC software.^{98,100} The focus is on thermodynamic conditions relevant to subsurface storage of H₂: pressures between 5 and 50 MPa, temperatures between 323.15 and 423.15 K, and NaCl concentrations varying between 0 and 2 molal. The reaction equilibria of CO₂-H₂O systems are not considered as bicarbonate concentrations are low.¹²³

The CFCMC method is based on an expanded ensemble and uses a coupling parameter λ to incrementally insert or remove molecules, leading to improved insertion/removal efficiency compared to single-step insertions and deletions.^{96–100,115} Simulations are performed using the *NPT* version of the CFCGE technique, developed by Poursaeidesfahani et al.,¹¹⁵ to determine the VLEs of mixtures consisting of H₂, CO₂, and NaCl brine. A single fractional molecule per component i , where i can be either CO₂, H₂O, or H₂, but not NaCl, is introduced in the simulations that is distinguishable from the whole molecules.¹¹⁵ Fractional molecules can be located in either of the two simulation boxes. The Lennard-Jones and electrostatic interactions of the fractional molecule with surrounding molecules are modulated by the coupling parameter $\lambda_i \in [0, 1]$. At $\lambda_i = 0$, the interactions resemble those of an ideal gas, while at $\lambda_i = 1$, interactions are fully scaled like those of a whole molecule. For the exact expressions of the scaled interactions the reader is referred to articles by Hens et al.⁹⁸ and Polat et al.¹⁰⁰ The details of the trial moves relevant for the CFCGE method: (1) molecule translations, (2) molecule rotations, (3) volume changes, and (4) hybrid insertions/deletions, are provided in the articles by Hens et al.,⁹⁸ Polat et al.,¹⁰⁰ and Rahbari et al.⁹⁹ To ensure that all values of λ_i are sampled in both simulation boxes, a weight function or a biasing function $W(\lambda_i, j)$ is introduced for species i in box j , where $j = 1$ or 2.^{98,100,115} The excess chemical potentials of each species i in box j in the *NPT* ensemble (μ_{ij}^{Ex}) equals^{66,93,98,100,115}

$$\mu_{ij}^{\text{Ex}} = -k_B T \ln \left(\frac{p_j(\lambda_i = 1)}{p_j(\lambda_i = 0)} \right) \quad (5)$$

where $p_j(\lambda_i)$ is the probability that a fractional molecule of species i samples a value of λ_i in box j , k_B is the Boltzmann constant, and T is the absolute temperature. In addition to assessing equilibrium between systems, the excess chemical potential aids in determining fugacity coefficients, crucial for describing phase-coexistence in mixtures,^{52,53} particularly used in equation of state-based thermodynamic modeling for phase

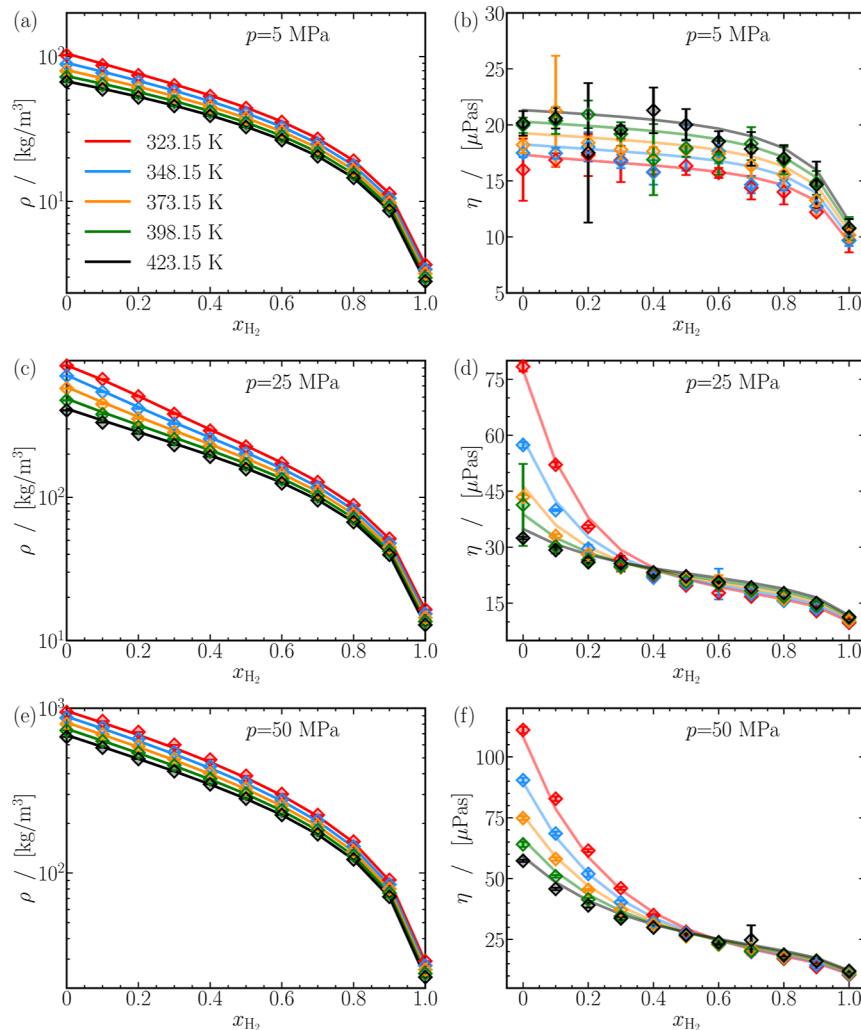


Figure 1. $\text{H}_2\text{-CO}_2$ mixture densities (ρ) and viscosities (η) at various pressures and temperatures. Computed properties (symbols) are compared to the REFPROP¹⁰⁸ data (solid lines). Uncertainties in simulation results are smaller than the symbol sizes. Lines are colored as per the legend in subfigure (a). Raw data on the densities and viscosities for all mixtures are provided in Tables S2 and S3 of the Supporting Information, respectively.

equilibria. Fugacity coefficients of species i (ϕ_i) are directly related to its excess chemical potential in the NPT ensemble as^{66,93}

$$\phi_i = \frac{1}{Z} \exp \left(\frac{\mu_i^{\text{Ex}}}{k_B T} \right) \quad (6)$$

where $Z = \frac{p \langle V \rangle}{N k_B T}$ is the compressibility factor for a mixture in the gas phase whose average volume equals $\langle V \rangle$. For further details of the CFC method the reader is referred to the articles by Hens et al.⁹⁸ and Polat et al.¹⁰⁰

In the systems of $\text{H}_2\text{-NaCl}$ brine and $\text{CO}_2\text{-NaCl}$ brine, 200 molecules of H_2 (or CO_2) in the gas-rich phase and 400 molecules of H_2O in the liquid-rich phase are initialized. For the ternary system of $\text{H}_2\text{-CO}_2\text{-NaCl}$, 100 molecules each of H_2 and CO_2 are initialized in the gas-rich phase, and 400 molecules of H_2O is initialized in the liquid-rich phase. 0, 7, and 15 ions of Na^+ and Cl^- , corresponding to NaCl concentrations of 0, 1, and 2 molal, are distributed randomly inside the H_2O -rich simulation box. A cutoff radius of 10 Å is applied for the LJ interactions, and analytic tail corrections are applied. Electrostatic energies are computed using the Ewald

summation¹²⁴ with a real-space cutoff of 10 Å and a damping parameter $\alpha = 0.32 \text{ \AA}^{-1}$ for both simulation boxes. The number of k -vectors in Fourier space is $k = 8$ in the liquid-rich box. To ensure convergence of electrostatic energies in the expansive gas-phase boxes, the maximum k -vectors are varied between 9 and 19. The relation between the real-space cutoff length, damping parameter α , and the maximum value of the k vectors is provided in the manual of Brick-CFCMC.^{98–100} These settings ensure that the electrostatic energies are computed with a relative precision of 10^{-6} .

Every cycle of a CFCGE simulation contains N_{Total} Monte Carlo (MC) trial moves, where N_{Total} is the total number of molecules. In the binary and ternary systems, molecule translations, rotations, and volume changes are selected with probabilities of 0.35, 0.24, and 0.01, respectively. Volume changes are computationally expensive since all configurational energies need recalculation based on the updated intermolecular distances after rescaling the simulation box. Consequently, volume changes are typically executed with a probability of 0.01.^{98,100} Changes of λ_i and molecule transfer moves (swapping and identity changes) are selected with probabilities of 0.2 each. The swapping of a fractional molecule

of species i between boxes is attempted if $\lambda_i < 0.3$, and the identity change of the fractional molecules is attempted only if $\lambda_i > 0.7$.¹¹⁵ The maximum displacements, rotations, volume changes, and λ changes are adjusted to obtain acceptance of ca. 50%. Molecule transfers involving salt ions Na^+ and Cl^- are excluded. For all simulations, an initialization phase lasting 10^4 cycles is simulated to remove overlaps between molecules. In an equilibration phase lasting 15×10^6 cycles, the weight functions $W(\lambda_j, j)$ are developed in each box, and a production phase lasting 10^6 cycles is used to calculate solubilities and fugacity coefficients (see eq 6). To obtain accurate values of solubilities and fugacity coefficients, 40 independent simulations are performed at each thermodynamic state point. The uncertainties (error bars) in the computation of solubilities and fugacity coefficients are estimated by dividing the 40 independent simulations into blocks of 5.³⁶ The solubilities of H_2 and CO_2 are determined as the ratio of the number of gas molecules to the total molecules in the liquid phase, with sodium and chloride ions considered separately. Liquid solubility in the gas phase is determined by the fraction of water molecules in the gas-rich phase.

3. RESULTS AND DISCUSSION

3.1. Densities and Compressibilities of $\text{CO}_2\text{-H}_2$ Mixtures. $\text{H}_2\text{-CO}_2$ mixture densities (ρ) at 5, 25, and 50 MPa are plotted as a function of the mole fraction of H_2 (x_{H_2}) in Figure 1a,c,e. The computed densities are compared with predictions from equations of state found in REFPROP.¹⁰⁸ Clearly, densities decrease monotonically and nonlinearly with the hydrogen content in the mixture. In Figure 1, densities computed from MD simulations closely match predictions from REFPROP,¹⁰⁸ typically within 5% at all thermodynamic state points. The relative deviations between the computed and predicted densities are shown in Figures S5–S7 of the Supporting Information.

The ratio of the densities of pure CO_2 and H_2 can vary between 20 and 35, considering all pressures and temperatures. The large density contrast between the pure components also impacts the mixture densities, as seen by the positive curvature ($\partial^2\rho/\partial x_{\text{H}_2}^2|_{p,T} > 0$) in Figure 1a,c,e, suggesting a strong influence of CO_2 content on the mixture densities. As expected, and as evident from Figure 1a,c,e, densities at a fixed pressure and mixture composition decreases with temperature. A ca. 31% increase in temperature (323.15 to 423.15 K), results in ca. 30% and ca. 40% reductions of densities of pure H_2 and CO_2 , respectively, at 5 and 50 MPa. Variations in $\text{H}_2\text{-CO}_2$ mixture densities with temperature lie between the bounds set by the pure components. It can be concluded that density and temperature have a linear-like relationship. A closer look at the vertical axis in Figure 1a,c,e, indicates that the density also increases with pressure. Barring the mixture at $x_{\text{H}_2} = 0$ and $T = 323.15$ K, $\rho(p)$ can be fitted to a second-degree polynomial with an error of up to ca. 10%. At $x_{\text{H}_2} = 0$ and $T = 323.15$ K, densities sharply increase until $p \approx 10$ MPa, followed by a more gradual rise. The proximity of this specific mixture to the critical point of CO_2 ($T_C = 304.15$ K, $p_C = 7.38$ MPa)¹²⁵ could explain the transition from gas-like behavior ($p \lesssim 10$ MPa) to fluid-like behavior ($p \gtrsim 10$ MPa). The reader is referred to Figures S1–S4 of the Supporting Information for additional plots of densities as functions of mole fraction of H_2 and pressure.

The compressibility factors (Z) of $\text{H}_2\text{-CO}_2$ mixtures are investigated to understand intermolecular interactions. Compressibilities vary nonlinearly with x_{H_2} , showing values both above and below unity. Excellent agreement between simulations and REFPROP predictions is observed for various pressures and temperatures. In general, mixtures rich in CO_2 exhibit attractive forces ($Z < 1$), while H_2 -enriched mixtures display repulsive forces ($Z > 1$). Temperature affects compressibilities differently at various pressures. Compressibilities tend to approach unity at low pressures and high temperatures. The behavior of compressibilities becomes more complex at higher pressures. Plots of compressibilities as a function of pressure and mole fraction of H_2 are provided in Figures S8–S10 of the Supporting Information.

To summarize, $\text{CO}_2\text{-H}_2$ mixture densities are dominated by the CO_2 content in the mixture. In mixtures with a high proportion of H_2 ($x_{\text{H}_2} \gtrsim 0.7$), repulsive interactions dominate, leading to densities lower than those of an ideal gas. Conversely, CO_2 -rich mixtures have higher densities due to attractive forces compared to ideal gas densities. Gas- and liquid-like behavior of $\text{H}_2\text{-CO}_2$ mixtures is observed depending on the pressure, temperature, and mixture composition. The densities and compressibilities computed from MD simulations and REFPROP¹⁰⁸ for all mixtures are tabulated in Table S2 of the Supporting Information.

3.2. Viscosities of $\text{CO}_2\text{-H}_2$ Mixtures. Viscosities (η) are usually independent of finite-size effects.^{116,118} The viscosities of various $\text{CO}_2\text{-H}_2$ mixtures as a function of x_{H_2} for 3 different pressures are shown in Figure 1b,d,f, while the remaining plots are displayed in Figures S12 and S13 of the Supporting Information. Similar to the mixture densities, the viscosities of $\text{H}_2\text{-CO}_2$ mixtures also show gas- and liquid-like behavior. Gas-like behavior is evident at 5 MPa, as depicted by viscosities within the range of a few μPas in Figure 1b.¹⁰⁰ Regardless of temperature, viscosities decrease monotonically with x_{H_2} . As the mixture becomes enriched with H_2 , the viscosities transition toward a more gas-like behavior, resulting in a gradual decrease of approximately 20% until $x_{\text{H}_2} \lesssim 0.8$, followed by a steeper drop of about 40%. By increasing the pressure to 25 and 50 MPa, specifically below 373.15 K, the behavior of viscosities differs from that shown in Figure 1b, indicating a liquid-like behavior. For example, at 25 MPa and 323.15 K, the viscosity decreases sharply by ca. 67% from about 75 μPas for pure CO_2 to around 25 μPas at $x_{\text{H}_2} = 0.5$. Subsequently, viscosities decrease nearly linearly with the mole fraction of H_2 . At 25 MPa and 423.15 K, $\eta(x_{\text{H}_2})$ resembles gas-like behavior. Viscosities are significantly impacted by the H_2 concentration in the $\text{H}_2\text{-CO}_2$ mixture, as indicated by the negative curvature of $\eta(x_{\text{H}_2})$ in Figure 1d,f ($\partial^2\eta/\partial x_{\text{H}_2}^2|_{p,T} < 0$).

The variation of viscosities with temperature further exemplifies the gas- and liquid-like behavior of the $\text{H}_2\text{-CO}_2$ mixtures. At 5 MPa and any fixed x_{H_2} , viscosities increase nearly linearly with temperature. An increase from 323.15 to 423.15 K results in a ca. 20% rise in the viscosities. The increase in viscosities with temperature reflects a gas-like behavior wherein the kinetic component of the viscosity exceeds the virial contribution due to molecular interactions, signifying the escalating influence of thermal motion on momentum transport in molecules. In contrast to gases, liquids experience a drop in viscosity with temperature.¹³ At 25 MPa

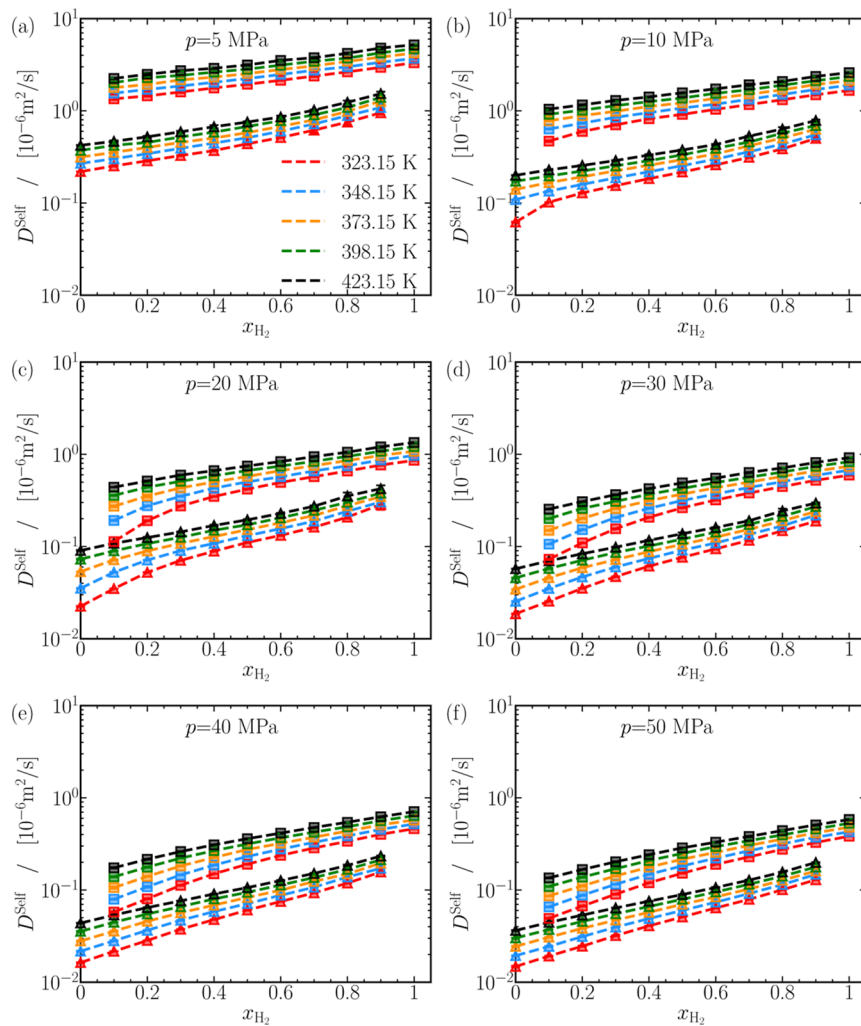


Figure 2. Self-diffusion coefficients (D_{Self}) of CO_2 (triangles) and H_2 (squares) in mixtures of CO_2 and H_2 , computed from MD simulations. The computed self-diffusion coefficients are plotted as a function of the mole fraction of H_2 in the mixture at various pressures. The uncertainties in the computed self-diffusion coefficients are smaller than the symbol sizes. The dashed lines act as guides to the eye. Lines are colored as per the legend in (a). Self-diffusivities of CO_2 and H_2 plotted on a linear scale are displayed in Figure S19a–f of the Supporting Information to aid comparison. The raw data of the self-diffusion coefficients of CO_2 and H_2 for all mixtures are provided in Table S3 of the Supporting Information.

in Figure 1d, for $x_{\text{H}_2} \lesssim 0.4$, viscosities decrease with temperature. While the same behavior is observed at 50 MPa, the liquid-like behavior is prominent for $x_{\text{H}_2} \lesssim 0.55$ in Figure 1f. Above a crossover concentration, $x_{\text{H}_2} \approx 0.4$ at 25 MPa and $x_{\text{H}_2} \approx 0.55$ at 50 MPa, viscosities increase with temperature due to the gas-like behavior of H_2 -enriched mixtures. The crossover concentration signals the transition from a liquid-like (or dense-gas like) behavior in CO_2 -enriched mixtures to a gas-like behavior in H_2 -enriched mixtures.

The viscosities can change significantly with pressure. Pure CO_2 shows a 4 to 5 times increase in viscosity upon increasing the pressure between 5 and 50 MPa, typical of dense gas-like behavior.¹¹ The addition of H_2 to the mixture substantially reduces viscosity. Pure H_2 maintains relatively low viscosities, with an insignificant dependence on pressure. The transition from gas-like to liquid-like behavior typically occurs within a pressure range of 30–40 MPa. These observations suggest that viscosity behavior is highly dependent on both pressure and composition, with clear distinctions between gas-like and liquid-like regimes. Plots for the viscosities as a function of

pressure for various mole fractions of H_2 are shown in Figures S14 and S15 of the Supporting Information.

Computed viscosities agree (on average) within 5% with REFPROP,¹⁰⁸ barring a few systems at 5 and 10 MPa. Deviations up to 28% are observed, noticeable from the large uncertainties at 5 MPa in Figure 1b, for instance, the data point at 373.15 K. The sparse intermolecular interactions in the gas phase lead to large fluctuations in p ¹¹¹ and require up to 40 ns to accurately compute viscosities. Another way to improve the accuracy of the computed viscosities is through more independent simulations. We refrained from conducting additional or longer simulations due to the satisfactory accuracy of the computed viscosities and the substantial computational costs associated with simulating the gas phase using MD. For instance, on a single core of an AMD7H12 2.6 GHz processor, simulating 1 ns of pure H_2 at 5 MPa and 423.15 K requires ca. 15 CPU hours, while pure CO_2 at 50 MPa and 323.15 K requires roughly 1 CPU hour. Computed and predicted values of viscosities for H_2 - CO_2 mixtures are tabulated in Table S3 of the Supporting Information.

3.3. Self-Diffusion Coefficients of CO_2 - H_2 Mixtures.

Self-diffusivities computed from MD simulations might need to

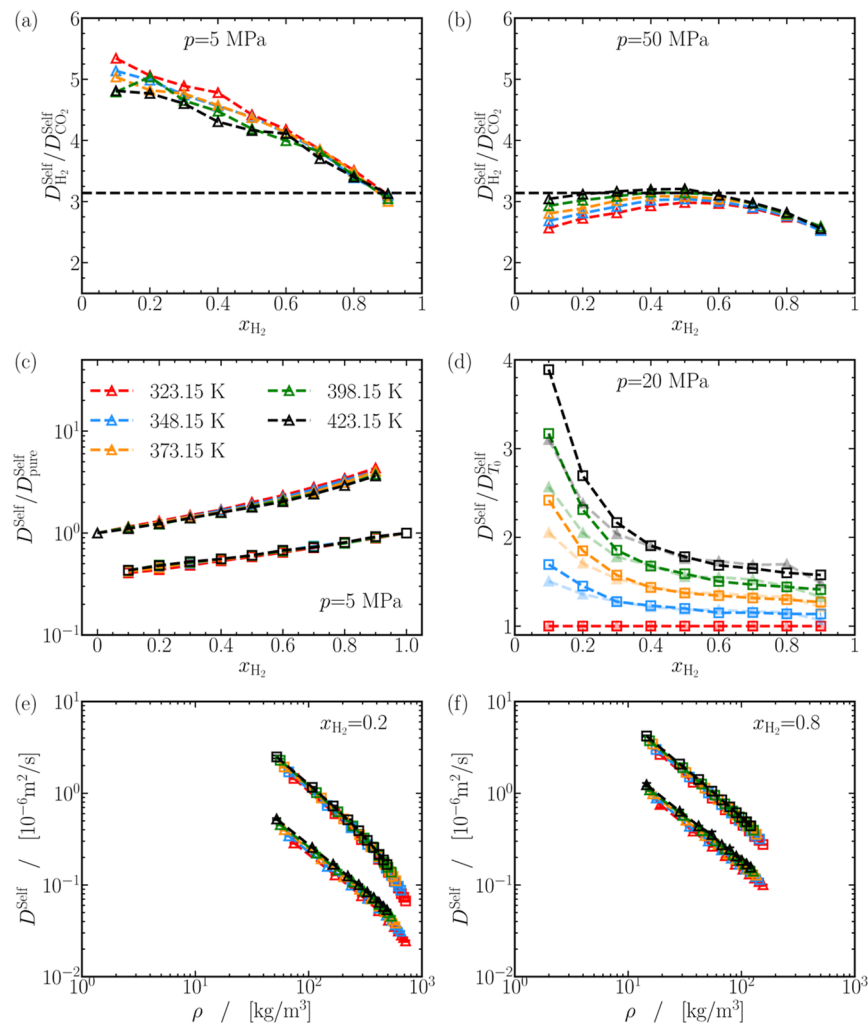


Figure 3. (a,b) Ratio of self-diffusivities of H₂ and CO₂ as a function of H₂ mole fraction at 5 and 50 MPa, respectively. The dashed line represents the ratio predicted by the Stokes–Einstein relation. (c) Comparison of the self-diffusivities of CO₂ (triangles) and H₂ (squares) in CO₂-H₂ mixtures with their values in pure fluids at the same temperature at 5 MPa. (d) Comparison of the self-diffusivities of CO₂ (triangles) and H₂ (squares) in CO₂-H₂ mixtures with their values at $T_0 = 323.15$ K at 20 MPa. (e,f) Self-diffusivities of CO₂ (triangles) and H₂ (squares) as a function of mixture densities at $x_{H_2} = 0.2$ and 0.8, respectively, with symbols colored according to the legend in (c). The ratios of self-diffusivities in (c) are displayed on a linearly scaled vertical axis in Figure S22 of the Supporting Information along with other pressures. Similarly, Figure S25 displays the densities and self-diffusivities in (e,f) plotted on linearly scaled horizontal and vertical axis. Figures S20–S25 of the Supporting Information contain additional plots for (a,b,d) at various pressures.

be corrected for finite-size effects,^{116–119} depending on the density of the system. Self-diffusivities are computed for systems containing 120, 250, 500, 1000, and 2000 molecules for 2 equimolar H₂-CO₂ mixtures: (1) 5 MPa, 423.15 K (33 kg/m³), and (2) 50 MPa, 323.15 K (389 kg/m³). For a system of 120 molecules, finite-size corrections for self-diffusivities in system (2) can reach up to 18% for CO₂ and around 7% for H₂, while in system (1), H₂ and CO₂ diffusivities remain unaffected by system size. The finite-size corrected self-diffusivity (D^{self}) of pure CO₂ at 2 MPa and 323.15 K ($2.2 \times 10^{-8} \text{ m}^2/\text{s}$) agreed within a percent of the value reported by Moulton et al.¹²⁶ Given the considerable variation in densities of H₂-CO₂ mixtures spanning nearly 2 orders of magnitude, finite-size effects are expected to affect the self-diffusivities of CO₂ and H₂ only at specific densities. Consequently, the Yeh–Hummer correction is applied when the correction term in eq 1 exceeds 1% of the uncorrected self-diffusivities. The reader is referred to Figures S17 and S18 for the plots of the finite-size effects.

The range between 10^{-8} and $10^{-6} \text{ m}^2/\text{s}$ for self-diffusivities in Figure 2, implies dense-gas and gas-like behavior of H₂-CO₂ mixtures.¹¹ As clearly shown in Figure 2, the self-diffusivities of H₂ are always larger than those of CO₂ at any pressure, temperature, or mixture composition by a factor between ca. 2.5 and 6. To explain why the self-diffusivities of H₂ exceed those of CO₂, the Stokes–Einstein (SE) relation^{11,127} is used. The SE equation links the self-diffusivity of a microscopic entity in liquid, viscosity, temperature, and effective radius (or a hydrodynamic radius, R^{eff}) as^{11,127}

$$D^{\text{self}} = k_B T / 6\pi\eta R^{\text{eff}} \quad (7)$$

Here, stick boundary conditions are assumed,^{11,127} resulting in a factor of 6π in the SE equation, in contrast to the 4π factor used with slip boundary conditions.^{11,127} It is also implicitly assumed that R^{eff} in eq 7 is unaffected by T .^{11,45} Treating CO₂ and H₂ as spherical entities with an R^{eff} equal to the bond length between carbon and oxygen (1.16 Å), and half the bond length between the two hydrogen atoms in H₂ (0.37 Å), the

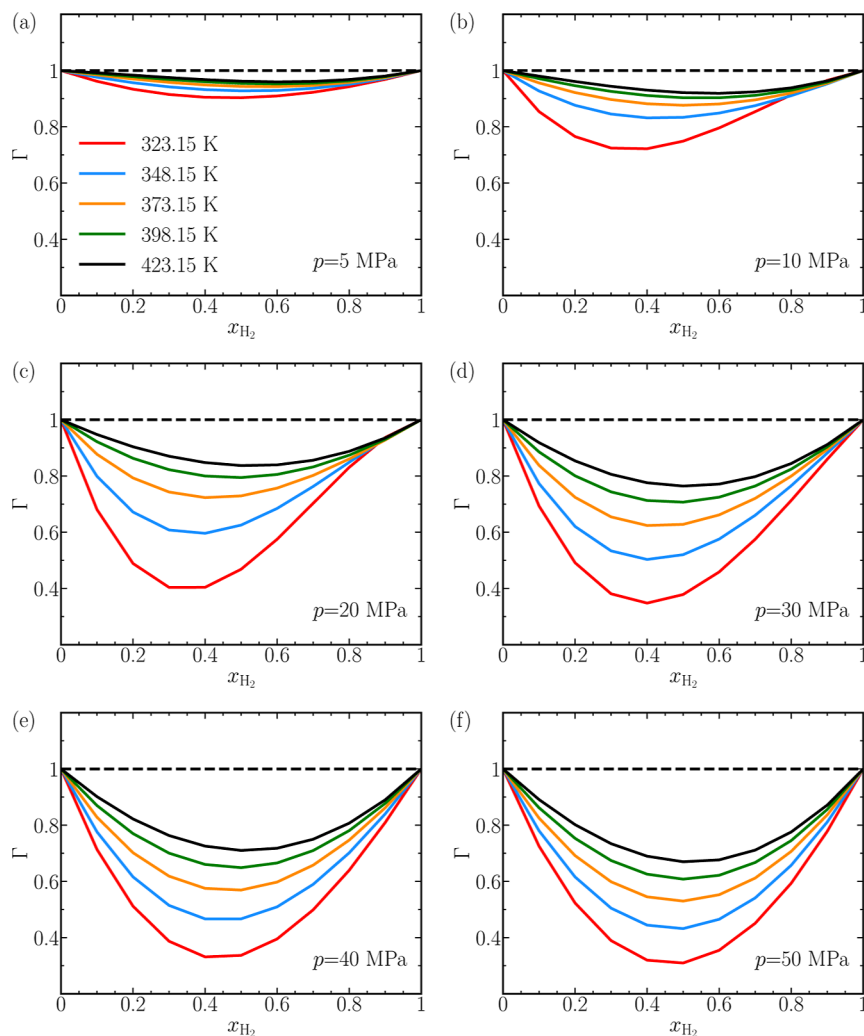


Figure 4. Thermodynamic factors (Γ) of $\text{CO}_2\text{-H}_2$ mixtures plotted as a function of the mole fraction of H_2 (x_{H_2}) for various pressures. Values of Γ are obtained from the Gibbs excess energies of $\text{H}_2\text{-CO}_2$ mixtures from REFPROP.¹⁰⁸ The dashed line corresponds to the ideal-mixture limit, where Γ equals 1. Lines are colored as per the legend in (a). The raw data of the thermodynamic factors of CO_2 and H_2 for all mixtures are provided in Table S3 of the Supporting Information.

ratio of their self-diffusivities as per eq 7 amounts to ca. 3.14, a value larger than unity. According to the SE relation, by the virtue of geometry, H_2 diffuses faster than CO_2 by roughly 3 times. In contrast to the expected ratio of ca. 3.14, according to the SE relation, the ratio of self-diffusivities for H_2 and CO_2 ranges from 2.5 to 6, indicating significant deviations. These deviations, as shown in Figure 3a, are particularly pronounced at 5 MPa, possibly due to the gas-like behavior of the mixtures, suggesting potential limitations in the applicability of the SE relation for gaseous systems. The agreement with the SE relation improves at larger pressures. For instance, Figure 3b indicates deviations less than 20% at 50 MPa, where the behavior of the mixtures resembles a liquid. The reader is referred to Figure S20a–d of the Supporting Information for similar plots between 10 and 40 MPa. While the SE equation provides a qualitative understanding of the self-diffusivities of CO_2 and H_2 , quantitative predictions may deviate due to (1) the incorrect assumption that R^{eff} remains constant with temperature, as also noted by Saric and colleagues,⁴⁴ and/or, (2) the oversimplified treatment of linear molecules like CO_2 and H_2 as spherical entities.

The impact of mole fraction of H_2 and temperature on the self-diffusivities is now discussed. As anticipated and shown in Figure 2a–f, self-diffusivities of CO_2 and H_2 increase as the proportion of H_2 increases in the mixture. This is because molecules can diffuse more in a gaseous medium than in liquid. To evaluate the effect of mole fraction of H_2 on self-diffusivities, the values of D^{self} for CO_2 and H_2 in $\text{H}_2\text{-CO}_2$ mixtures are compared with corresponding values in pure fluids, as shown for the diffusivities at 5 MPa in Figure 3c. Adding H_2 to the mixture can lead to a nearly exponential rise in the self-diffusivities of both CO_2 and H_2 , with a maximum increase of approximately 2 to 4 times. A similar exponential increase in the self-diffusivities is observed also at other pressures, as shown in Figures S21 and S22 of the Supporting Information.

As anticipated, increasing temperature leads to larger self-diffusivities of H_2 and CO_2 , as seen in Figure 2a–f due to the more gas-like nature of systems at larger T . The ratio of self-diffusivities of H_2 and CO_2 relative to their values at 323.15 K is plotted in Figure 3d at 20 MPa. The self-diffusivity of CO_2 and H_2 increases up to 300% at $x_{\text{H}_2} = 0.1$, while a modest increase up to 60% is observed for both species at $x_{\text{H}_2} = 0.9$. A

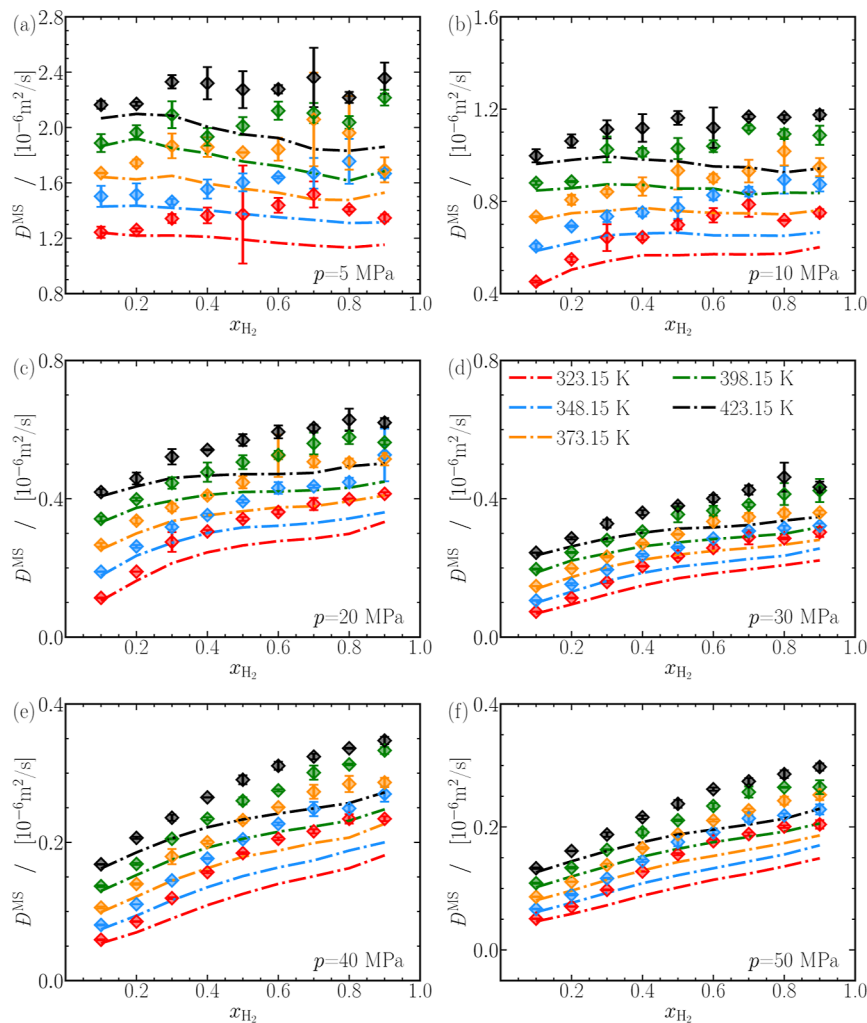


Figure 5. Finite-size-corrected Maxwell–Stefan diffusion coefficients as a function of the mole fraction of hydrogen (x_{H_2}). The dashed-dotted lines are predictions from the Darken relation (eq 3, where the self-diffusion coefficients for CO_2 and H_2 are taken from Figure 2). Lines are colored as per the legend in (d). The raw data of the Maxwell–Stefan diffusion coefficients of CO_2 and H_2 mixtures are provided in Table S3 of the Supporting Information.

similar trend is observed at all pressures, barring 5 MPa, where the self-diffusivity of both species increases by a maximum of ca. 100% at $x_{H_2} = 0.1$, but at $x_{H_2} = 0.9$, the increase is between 50 and 60%. At 5 MPa, however, self-diffusivities of H_2 and CO_2 increase by ca. 60% at all mixture compositions, exhibiting a linear-like response to temperature. It can be concluded that self-diffusivities of H_2 and CO_2 in mixtures rich in H_2 ($x_{H_2} \gtrsim 0.7$) respond similarly to temperature at all pressures. For mixtures rich in CO_2 the response of self-diffusivities to temperature varies depending on the pressure, indicating a complex behavior. This complexity may be associated with the proximity of CO_2 to the supercritical phase ($T_C = 304.15 \text{ K}$, $p_C = 7.38 \text{ MPa}$).¹²⁵

The self-diffusivities of CO_2 and H_2 increase with the mole fraction of H_2 and temperature but decrease with pressure. Conversely, mixture densities decrease with the mole fraction of H_2 and temperature while increasing with pressure. The contrasting responses of self-diffusivities and densities imply a possible correlation between the two quantities. Figure 3e,f show the variation of self-diffusivities for CO_2 and H_2 with density at $x_{H_2} = 0.2$ and 0.8, respectively. A linear-like relationship, displayed on a log–log scale, between the self-

diffusivities of both H_2 and CO_2 and density is apparent. A linear fit is calculated to best describe this relationship at all mixture compositions. The average value of the slopes of the linear fits for the case of CO_2 is -1.00 ± 0.05 and -1.1 ± 0.1 for H_2 . Minor deviations from the calculated slope of around -1 are found for ρ exceeding ca. 400 kg/m^3 , in Figure 3e. Similar deviations in the slopes are also observed for pure CO_2 for $\rho \gtrsim 500 \text{ kg/m}^3$. Barring these exceptions, it can be concluded that the self-diffusivities for CO_2 and H_2 are inversely proportional to the mixture density. When comparing Figure 3e,f, a significant vertical shift of the data points is observed, along with a minor horizontal shift. The shifts imply dependencies of self-diffusivities not only on the density but also on x_{H_2} and T . It appears improbable to establish a master equation linking self-diffusivities solely to densities. Studies by Van Loef¹²⁸ and Harris and Trappeniers¹²⁹ studying pure liquids, found that self-diffusivities are functions of density and temperature. In a binary mixture, an extra thermodynamic degree of freedom, the mole fraction of a component, must be considered alongside density and temperature to fully describe self-diffusivities. Establishing a function correlating self-diffusivities to density, temperature, and x_{H_2} will require

additional efforts. Currently, no experimental data are available to compare the computed self-diffusivities in H₂-CO₂ mixtures. Additional plots of self-diffusivities as a function of ρ are shown in Figure S24a–d. The computed self-diffusivities in H₂-CO₂ mixtures are tabulated in Table S3 of the Supporting Information.

3.4. Thermodynamic Factors for Diffusion for CO₂-H₂ Mixtures. Figure 4 shows the thermodynamic factors calculated from the Gibbs excess energies obtained from REFPROP.¹⁰⁸ The values of Γ for the thermodynamic states considered in this work are positive and vary between 0.25 and 1. Positive values of Γ signify that the mixtures are thermodynamically stable and do not undergo phase separation.¹⁰ A notable deviation from unity in the values of Γ for the CO₂-H₂ mixtures suggests highly nonideal behavior. Γ of a binary system must approach unity when approaching the pure-component limit.^{10,12}

At a fixed mixture composition, the values of Γ tend to decrease with pressure. For instance, in Figure 4, for an equimolar mixture of CO₂-H₂ the value of Γ for the mixture drops from ca. 0.9 at $p = 5$ MPa (Figure 4a) to ca. 0.3 at $p = 50$ MPa (Figure 4f). This holds true for the values of Γ at other mixture compositions. For a fixed mixture composition, the value of Γ approaches 1 as the temperature rises from 323.15 K to 423.15 K, regardless of the pressure. For instance, at $p = 50$ MPa (Figure 4f), the value of Γ increases from ca. 0.3 at $T = 323.15$ K to ca. 0.7. At a specific temperature and pressure, the values of Γ exhibit a slight asymmetry ca. $x_{\text{H}_2} = 0.5$, see Figure 4c ($p = 20$ MPa). The thermodynamic factors of all CO₂ and H₂ mixtures considered in our study are tabulated and displayed in Table S3 of the Supporting Information.

3.5. MS and Fick-Diffusion Coefficients for CO₂-H₂ Mixtures. MS diffusivities computed from MD simulations require finite-size corrections.^{116–119} To investigate finite-size effects in MS diffusivity calculations and to confirm the validity of eq 2 for our systems, equimolar H₂-CO₂ mixtures at 50 MPa and 323.15 K (389 kg/m³) consisting of 120, 250, 500, 1000, and 2000 molecules were chosen. Both methods, extrapolation of the line fitted to the MS diffusivities up to $N_{\text{tot}} \rightarrow \infty$ and the prediction from eq 2, agreed within 3%. The finite-size correction to the MS diffusivity for the system of 120 molecules was ca. 20%, underscoring the significance of finite-size effects in the computation of MS diffusivities. Consequently, the correction suggested in eq 2 is applied if it exceeds 1% of the computed MS-diffusivities. The reader is referred to Figure S27 for the plots of the finite-size effects in MS diffusivities.

Figure 5a–f shows the finite-size corrected MS diffusivities (D^{MS}) for various CO₂-H₂ mixtures, compared to the Darken prediction from eq 3. Finite-size corrected self-diffusivities of CO₂ and H₂ are used to compute the Darken predictions. The Darken prediction underestimates the computed MS diffusivities for the mixtures considered in our study. The maximum deviations between eq 3 and the computed MS diffusivities can reach ca. 30% around $x_{\text{H}_2} \approx 0.7$, while a minimum deviation of about 5% occurs at $x_{\text{H}_2} \approx 0.1$.

The significant deviations between the computed MS diffusivities and Darken predictions imply a significant nonideality of the H₂-CO₂ mixtures. Since the thermodynamic factor (Γ) reflects the nonideality of the mixture, it is valuable to explore the potential correlation between $B^{\text{MS}} - D^{\text{Darken}}$ and Γ , as suggested by Wolff et al.¹²² Figure 6a shows the relative

deviation of the MS diffusion coefficient from the Darken relation as a function of the thermodynamic factor, for all mixtures considered in our study. The Moggridge correlation^{122,130–134} when recast into a suitable form

$$\frac{D^{\text{MS}}}{D^{\text{Darken}}} = \Gamma^{-0.36} \rightarrow \frac{B^{\text{MS}} - D^{\text{Darken}}}{D^{\text{Darken}}} = \Gamma^{-0.36} - 1 \quad (8)$$

reasonably describes the relative deviation of D^{MS} from D^{Darken} and the thermodynamic factor, with the best agreement achieved at low temperatures. Figure 6b helps carefully assess

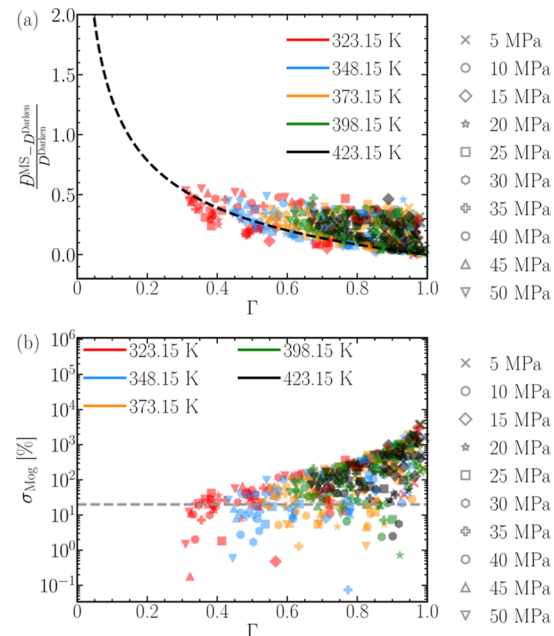


Figure 6. (a) Relative differences between the Darken relation and the computed MS diffusivities plotted as a function of the thermodynamic factor Γ for all pressure, temperature, and mixture compositions. The dashed line is the Moggridge correlation,^{122,130–134} see eq 8. The symbols code for the pressure and the colors code for the temperature. For example, a blue star would correspond to 20 MPa and 348.15 K. (b) Relative deviations, in percentage, of the symbols in (a) from the Moggridge correlation (σ_{Mog}). The dashed line corresponds to a deviation of 20% to aid visual comparison. The percentage deviation extends across 5 orders of magnitude.

the performance of the Moggridge correlation^{122,130–134} by showing the percentage deviations between the symbols and the dashed line in Figure 6a. The deviations in Figure 6b are within 20% when describing mixtures below 348.15 K and above 40 MPa. In other words, the deviation between the computed MS diffusivities and the Darken relation is accurately captured in the liquid-like phase. The Moggridge correlation becomes less accurate when considering H₂-CO₂ mixtures at high temperatures and low pressures. For instance, the black cross representing 5 MPa and 423.15 K exhibits the maximum deviation. To conclude, Moggridge correlation can be advantageous in predicting the deviation between the computed MS diffusivities and the Darken relation for mixtures behaving as liquids. In summary, knowing the self-diffusivities of H₂ and CO₂ and the thermodynamic factor can facilitate the prediction of D^{MS} of the mixture with an accuracy of approximately 20% for mixtures between 40 and 348.15 MPa.

Fick diffusivities for CO₂-H₂ mixtures are the products of the MS diffusivities and the thermodynamic factors, as shown in eq

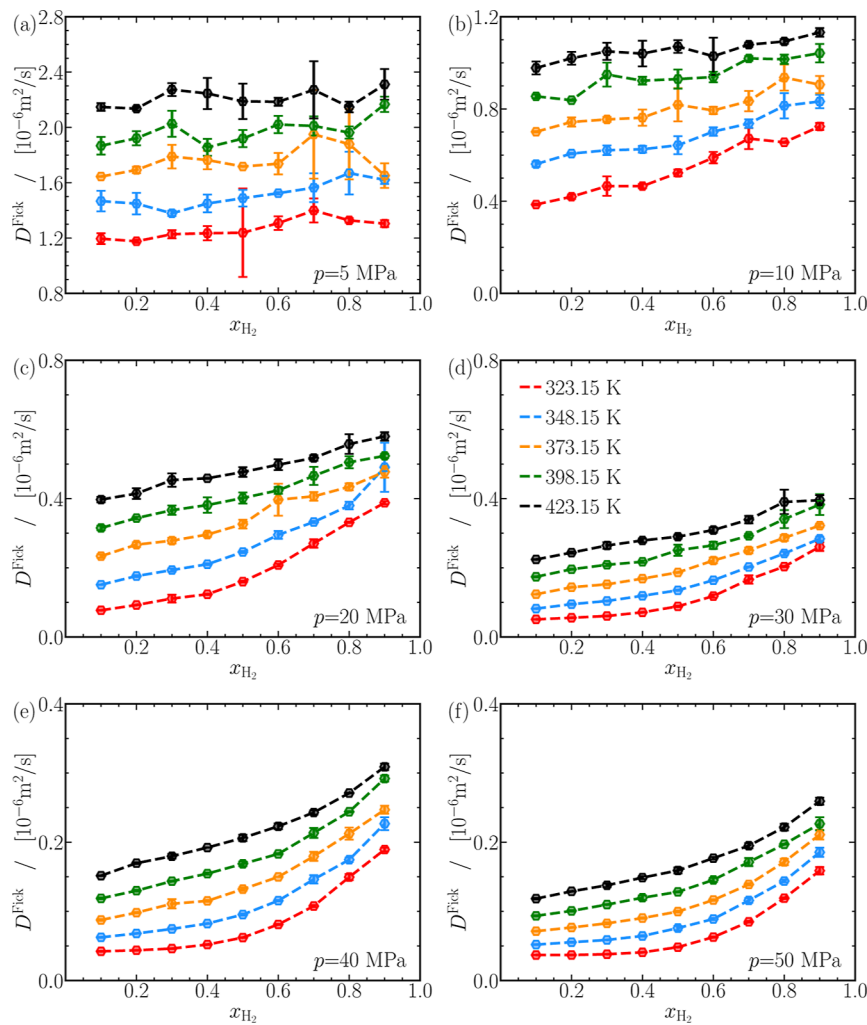


Figure 7. Finite-size-corrected Fick diffusion coefficients as a function of the mole fraction of hydrogen (x_{H_2}). Lines are colored as per the legend in (d). The dashed lines act as guides to the eye. The raw data of the Fick diffusion coefficients of CO_2 and H_2 for all mixtures are provided in Table S3 of the Supporting Information.

4. Similar to the self- and MS diffusivities, finite-size corrections are disregarded if the corrections are less than 1% of the computed values, as shown in eq 4. Figure 7a–f shows the Fick diffusivities as a function of the mole fraction of hydrogen. The statistical uncertainties in the computed Fick diffusivities are noticeable, particularly below ca. 10 MPa, as shown in Figure 7a–c. This increased uncertainty, such as at 5 MPa, 323.15 K, and $x_{\text{H}_2} = 0.5$, is attributed to sparse intermolecular collisions in the gas phase, leading to slow convergence toward diffusive behavior of the cross-correlation of mean-squared displacements of H_2 and CO_2 . To enhance accuracy, more independent simulations could be performed, but we refrained from doing so due to the significant computational costs associated with gas-phase MD simulations. The Fick diffusivities computed for all pressures, temperatures, and mixture compositions vary between $10^{-8} \text{ m}^2/\text{s}$ at 50 MPa and $10^{-6} \text{ m}^2/\text{s}$ at 5 MPa, indicating dense-gas/liquid-like behavior at high pressures and gas-like behavior at low pressures. In contrast to the smooth increase observed for self-diffusivities of H_2 and CO_2 in Figure 2a–f, the behavior of Fick diffusivities varies as the content of H_2 increases in the mixture depending on the pressure. At 5 MPa in Figure 7a, Fick diffusivities exhibit minimal dependence on mixture

composition, whereas at 50 MPa in Figure 7f, they can increase by 3 to 4 times with higher H_2 enrichment in the mixture. The variation in Fick diffusivities contrasts with the consistent increase observed in the self-diffusivities of H_2 and CO_2 with the content of H_2 in the mixture.

In general, temperature elevation increases Fick diffusivities regardless of mixture composition or pressure. The extent of this increase, however, varies for different mixtures. Notably, for mixtures abundant in H_2 ($x_{\text{H}_2} = 0.9$), Fick diffusivities consistently double when the temperature rises from 323.15 to 423.15 K across all pressures. Conversely, for mixtures rich in CO_2 ($x_{\text{H}_2} \lesssim 0.2$), the increase ranges between ca. 100% (at 5 MPa) and ca. 300% (at 20 MPa) depending on pressure, emphasizing the significant impact of temperature on Fick diffusivities, particularly for CO_2 -rich mixtures. The effect of temperature on Fick diffusivities aligns with trends seen in the self-diffusivities of both CO_2 and H_2 .

3.5.1. Prediction of Fick Diffusion Coefficients Using Kinetic Theory, Fuller Correlation, the Corresponding States Principle, and Moggridge's Correlation. Due to the lack of experimental data or a specific theory to predict Fick diffusivities in CO_2 - H_2 mixtures at pressures larger than atmospheric pressure, the computed diffusivities are compared

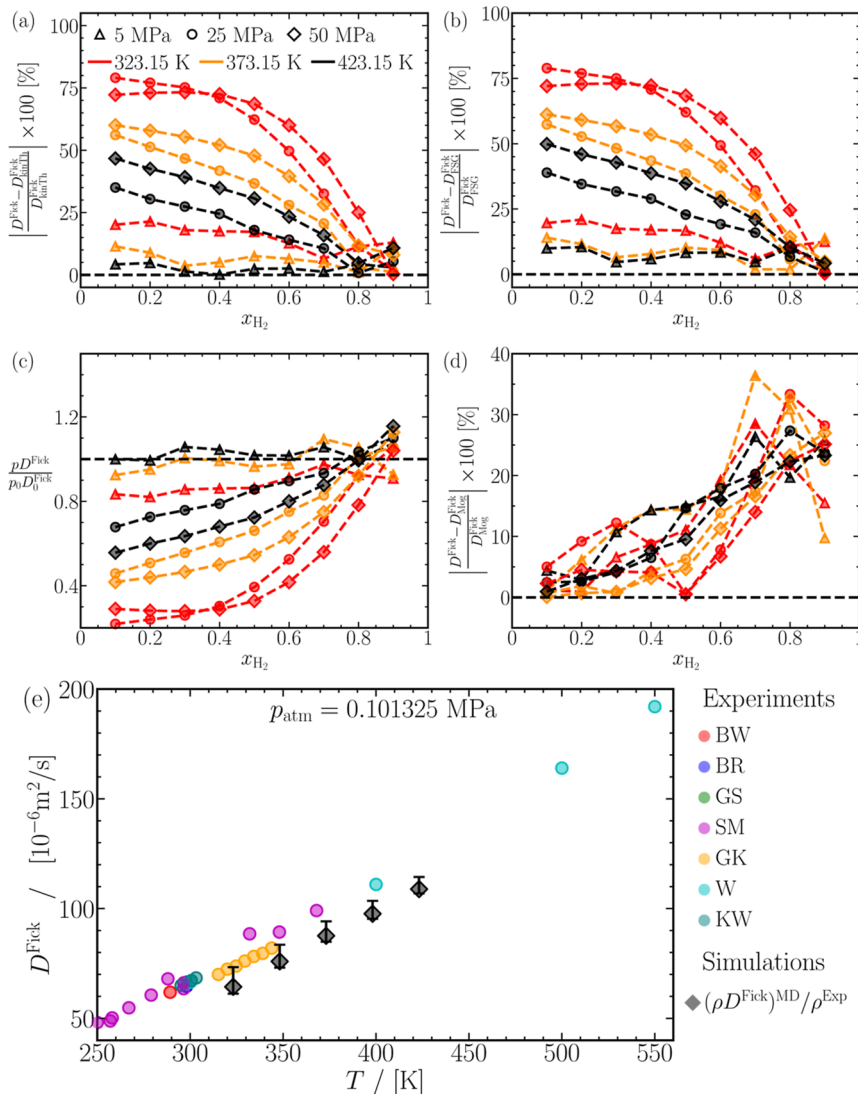


Figure 8. Absolute relative deviations between Fick diffusivities computed from MD simulations and predictions using (a) kinetic theory,^{16–18} (b) FSG correlation,^{11,30–32} (c) corresponding states principle¹¹ for pD_{Fick} , where $D_0^{\text{Fick}} = D_{\text{Fick}}(p_0 = 0.1 \text{ MPa})$ is evaluated using kinetic theory,^{16–18} and (d) Moggridge correlation^{122,130–134} for DH^{MS} . (e) Experimentally measured Fick diffusivities of $\text{CO}_2\text{-H}_2$ mixtures at atmospheric pressure (p_{atm}) compared to Fick diffusivities extrapolated from MD simulations of equimolar $\text{CO}_2\text{-H}_2$ mixtures at 5 MPa and temperature T using the principle of corresponding-states¹¹ (also see eq 11). The asymmetric error bars indicate Fick diffusivities calculated using $x_{\text{H}_2} = 0.1$ and 0.9. Experiments by Boardman and Wild¹⁴⁵ (BW), Boyd et al.¹⁶⁸ (BR), Giddings and Seager¹⁶⁵ (GS), Saxena and Mason¹³⁶ (SM), Gavril et al.¹³⁵ (GK), Weissman¹³⁷ (W), and Kestin et al.¹⁶¹ (KW) are chosen for comparison.

to various models: (1) Chapman Enskog expression from kinetic theory,¹¹ (2) the correlation established by Fuller, Schettler, and Giddings (FSG),^{30–32} (3) the corresponding states principle,¹¹ and (4) predictions from MS diffusivities using Moggridge's correlation.^{122,130–134}

Figure 8a shows the relative deviations of the computed Fick diffusivities from the kinetic theory expression of Chapman and Enskog. It can be expected that kinetic theory effectively predicts Fick diffusivities when mixtures behave ideally, typically observed at low pressures, high temperatures, and in mixtures rich in H_2 . In line with this expectation, a close agreement within 5% is evident at 423.15 K and 5 MPa for all mixtures. Below 423.15 K, predictions of kinetic theory are accurate within ca. 10% at 373.15 K and ca. 20% at 323.15 K. The computed Fick diffusivities of mixtures rich in H_2 ($x_{\text{H}_2} \gtrsim 0.8$) can be predicted within 15% regardless of the pressure. As anticipated, a severe loss of accuracy in kinetic theory (up to

75%) is observed for CO_2 -rich mixtures ($x_{\text{H}_2} \lesssim 0.5$) at 25 and 50 MPa, regardless of the temperature. In conclusion, predictions of D_{Fick} from kinetic theory are reliable up to ca. 20% at pressures of 5 MPa for $\text{CO}_2\text{-H}_2$ mixtures.

The FSG correlation^{30–32} is a widely used method for estimating Fick diffusivities.^{30–32} The relative deviations between the computed and predicted diffusivities of $\text{CO}_2\text{-H}_2$ mixtures are shown in Figure 8b. Figure 8a,b exhibits striking similarity, indicating predictive capabilities of the FSG correlation comparable to the kinetic theory. This is not surprising, provided that Fuller's empirical relation is based on the Chapman and Enskog expressions from kinetic theory. It can be concluded that the kinetic theory and Fuller correlation can reliably estimate the Fick diffusivities within 25% in $\text{H}_2\text{-CO}_2$ mixtures up to 5 MPa and temperatures between 323.15 and 423.15 K. For pressures below ca. 5 MPa and temperatures above ca. 423.15 K, the accuracy of predicted Fick diffusivities

from kinetic theory, and the Fuller correlation are expected to increase, consistent with findings in the literature.^{11,13}

To test if accurate predictions of Fick diffusivities can be made at larger pressures, the performance of the corresponding state principle is examined. The ratio $pD^{\text{Fick}}/p_0D_0^{\text{Fick}}$ is evaluated at all thermodynamic state points, where D_0^{Fick} is the Fick diffusivity evaluated at a reference pressure $p_0 = 0.1$ MPa and the corresponding temperature T . When the ratio equals unity, D^{Fick} at any pressure and temperature can be predicted since the normalization factor is readily accessible. Figure 8c shows that the ratio is within 3% of unity at 5 MPa and 423.15 K. Like kinetic theory and FSG correlation, predictions are less accurate (deviations up to ca. 40%) at high pressures for mixtures rich in CO₂. Conversely, mixtures rich in H₂ ($x_{\text{H}_2} \gtrsim 0.8$) agree within 15–20% with kinetic theory and Fuller correlation. Rather than using pressure p to assess the ratio $pD^{\text{Fick}}/p_0D_0^{\text{Fick}}$, an alternative approach is to use density ρ , as illustrated in Figure S31 of the Supporting Information. While the performance of the corresponding states principle remains qualitatively similar, there is a marginal improvement of ca. 10% in the prediction of Fick diffusivities at 5 MPa, as shown in Figure S31 of the Supporting Information. In a nutshell, predicting Fick diffusivities is feasible through the kinetic theory, FSG correlation, or the corresponding states principle, specifically for mixtures at low pressures and high temperatures or enriched with hydrogen.

Due to the superior performance of Moggridge's correlation, specifically at high pressures and low temperatures, this empirical method could be advantageous for predicting Fick diffusivities at these conditions (see Figure 6a,b). By combining eqs 4 and 8, Moggridge's correlation can be extended to describe Fick diffusivities as

$$D_{\text{Mog}}^{\text{Fick}} = DH_{\text{Mog}}^{\text{MS}} \Gamma = D^{\text{Darken}} \Gamma^{0.64} \quad (9)$$

As anticipated, in Figure 8d, the Fick diffusivities predicted using eq 9 closely match the computed values, staying within 5% at 25 and 50 MPa for temperatures of 323.15 and 348.15 K. For CO₂-rich mixtures ($x_{\text{H}_2} \lesssim 0.2$), the computed and predicted Fick diffusivities deviate by less than ca. 5%, irrespective of pressure and temperature. In sharp contrast, for H₂-rich mixtures ($x_{\text{H}_2} \gtrsim 0.7$) and mixtures at low pressures, deviations from the computed Fick diffusivities can reach approximately 35%.

In summary, Chapman and Enskog's kinetic theory, FSG correlation, and the corresponding states principle perform well for ideal-gas-like mixtures. Fick diffusivities for H₂-CO₂ mixtures below 5 MPa can be accurately predicted within 5–10%. These kinetic theory-based approaches also demonstrate good performance for mixtures rich in H₂ ($x_{\text{H}_2} \gtrsim 0.8$), with an accuracy of approximately 15–20%. Deviations can be as high as 75% when predicting Fick diffusivities of nonideal mixtures. For higher pressures and CO₂-rich mixtures ($x_{\text{H}_2} < 0.5$), using Moggridge's correlation for MS diffusivities yields Fick diffusivities accurate to within 5–10%. Values of MS and Fick diffusivities for all CO₂ and H₂ mixtures considered in our study are provided in Table S3 of the Supporting Information.

3.5.2. Comparison of MD-Computed Fick Diffusivities with Experiments. We aim to (indirectly) compare the Fick diffusivities of CO₂-H₂ mixtures from MD simulations to existing experiments at $p_{\text{atm}} = 1$ atm (see Table 1). Computing Fick diffusivities at atmospheric pressure using MD simulations

is possible but impractical due to the severe computational demands accompanying gas phase simulations.

The principle of corresponding states can indirectly compute Fick diffusivity at an unknown pressure, in our case, the atmospheric pressure, by extrapolating known data from a reference pressure.^{11,13} For comparison with experiments, Fick diffusivities computed from MD simulations at a reference pressure of 5 MPa are used to estimate mutual diffusivities at atmospheric pressure. Comparison of the computed Fick diffusivities at 5 MPa with those estimated using kinetic theory at 0.1 MPa reveals that the product of pressure (or density) and mutual diffusivities remains nearly constant (see Figure 8e), with deviations of approximately 20%. This trend is consistent when analyzing densities instead of pressures, showing agreement within 10%, as shown in Figure S31 of the Supporting Information. The principle of corresponding states for the product of density and Fick diffusivity offers a practical approach to extrapolating computed Fick diffusivities to conditions of experimental relevance. The Chapman-Enskog expression for mutual diffusivity, denoted as D_{AB} , of rigid spheres with unequal masses is given by^{11,17,18}

$$D_{\text{AB}} = \frac{3}{16} \sqrt{\frac{2\pi k_B T}{M_{\text{AB}}}} \frac{1}{n\pi\sigma_{\text{AB}}^2 \Omega(T)} \quad (10)$$

where D_{AB} [m² s⁻¹] is the mutual diffusivity of the A-B mixture, M_{AB} is the reduced mass of A and B, k_B is the Boltzmann constant, n [m⁻³] is the number density, σ_{AB} [m] is the characteristic length of the intermolecular force law, and $\Omega(T)$ is the temperature-dependent collision integral for diffusion. Multiplying both sides of eq 10 by $nM_{\text{mix}}/N_{\text{Av}}$, where $M_{\text{mix}} = M_Ax_A + m_Bx_B$ is the molecular mass of the mixture in kg·mol⁻¹, and N_{Av} [mol⁻¹] is the Avogadro number, which allows us to express it as

$$\rho D_{\text{AB}} = f(T, M_{\text{mix}}) \quad (11)$$

The functional form of eq 11 suggests that the product of density and Fick diffusivity can be equated between two thermodynamic states under the same temperature and mixture composition, as M_{mix} depends on the mole fraction of species A. Although eq 10 assumes spherical molecules, the equation has been shown to be effective at low pressures, irrespective of the shape of the molecules.^{11,13,17}

From Figure 8e, we observe good agreement (within ca. 15%) between the Fick diffusivities predicted from the principle of corresponding states using eq 11 (filled diamonds) for an equimolar mixture composition, and experimental data by Gavril et al.,¹³⁵ Saxena and Mason,¹³⁶ and Weissman.¹³⁷ The asymmetric error bars associated with each symbol in Figure 8e, representing the values of D^{Fick} calculated using eq 11 with mixture compositions of $x_{\text{H}_2} = 0.1$ and 0.9, respectively, imply a weak dependence of Fick diffusivities on mixture concentration. Accounting for this variability in the Fick diffusivities by choosing different mixture compositions enhances agreement with the experiments (between ca. 1 and 5%). Leveraging the close agreement between MD computed densities and REFPROP¹⁰⁸ predictions (see Figures 1 and S5–S7 of the Supporting Information), Fick diffusivities can be evaluated at experimentally relevant conditions for mixture compositions of 0.001 and 0.999, yielding consistent results. Experimental measurements used in Figure 8e are not corrected for composition effects, known to affect diffusivities by ca. 5%,¹⁹ potentially influencing agreement between MD

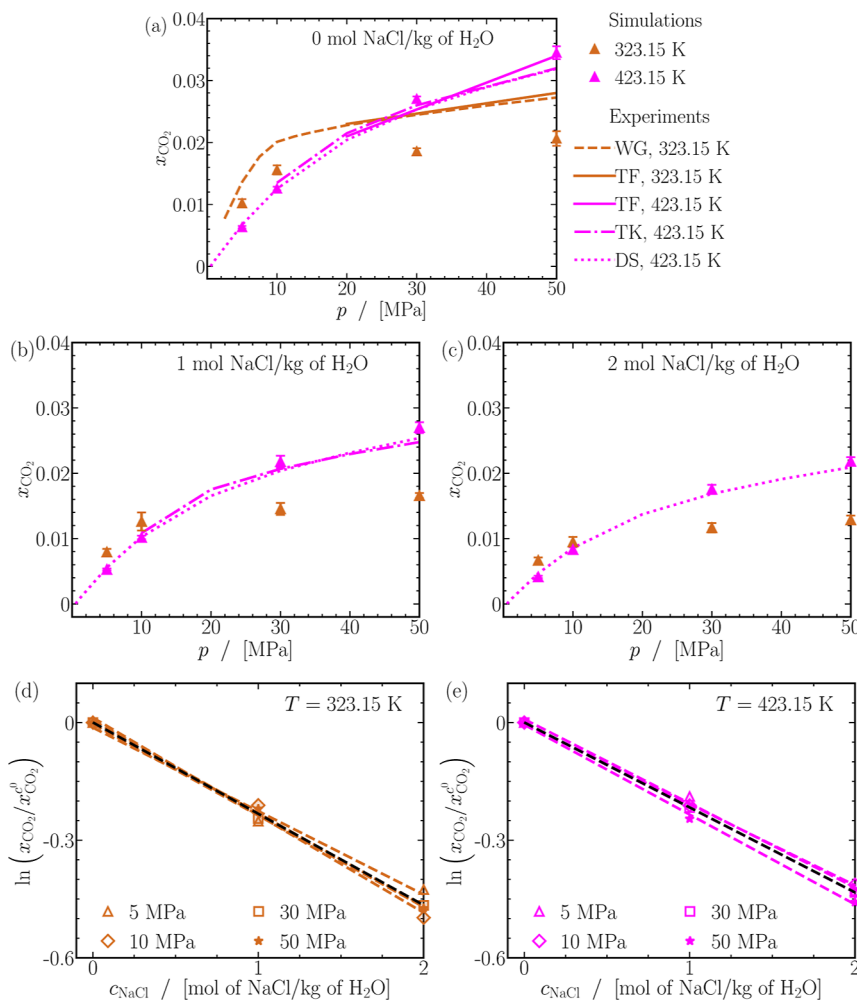


Figure 9. (a–c) CO_2 solubilities in NaCl brine computed from MC simulations (symbols) compared to experiments (lines) for varying brine concentrations. Experimental studies of Weibe and Gaddy (WG),¹⁶⁹ Tödheide and Frank (TF),¹³⁸ Takenouchi and Kennedy (TK),^{170,171} and Duan and Sun (DS)^{56,88} are considered for the comparison. (d,e) Reduction in the solubility of CO_2 as a function of NaCl concentration in brine. The logarithm of the ratio of CO_2 solubility in brine to its solubility in pure water is plotted as a function of NaCl concentration. Linear fits to the data are shown as dashed lines. The raw data of the solubilities are provided in Table S4 of the Supporting Information.

simulations and experimental measurements. Using the product of pressure and Fick diffusivity in eq 11 yields similar conclusions. In summary, MD simulations provide reliable estimates of Fick diffusivities at conditions relevant to atmospheric pressure and temperatures between 323.15 and 423.15 K.

3.6. Phase Equilibria of CO_2 -NaCl Brine Mixtures. The solubilities of CO_2 in pure water and NaCl brine at 323.15 and 423.15 K between 5 and 50 MPa and for salt concentrations of 1 and 2 mol of NaCl/kg of H_2O . At 323.15 K in Figure 9a–c, CO_2 undergoes a significant linear-like increase in solubility within the liquid-rich phase up to $p \lesssim 10$ MPa. Beyond this pressure, the solubility continues to increase linearly, albeit more gradually. The distinct slopes in these two regions reflect a transition from a gas-like to a liquid-like behavior of CO_2 . At 423.15 K, x_{CO_2} varies almost quadratically with pressure. As $p \rightarrow 0$, extrapolation of x_{CO_2} shows that the solubility of CO_2 also approaches 0, in agreement with the definition of the Henry regime. In general, insensitive to the concentration of NaCl in H_2O , increasing pressure from 5 to 50 MPa results in a 2-fold increase in x_{CO_2} at 323.15 K and a 5-fold increase in x_{CO_2} at 423.15 K. The effect of temperature on the solubility of CO_2 is

nontrivial. Beyond a certain threshold pressure p_{Th} , the solubility of CO_2 in the NaCl brine increases with temperature. Below p_{Th} , temperature has the opposite effect, leading to a decrease in CO_2 solubility. This threshold pressure appears to depend on the NaCl concentration in H_2O .

Solubilities of CO_2 in NaCl brine computed from simulations are compared to experimental data obtained from Weibe and Gaddy (WG),¹³⁷ Takenouchi and Kennedy (TK),³³ Duan and Sun (DS),⁵⁶ and Tödheide and Frank (TF).¹³⁸ In Figure 9a–c the computed solubilities at 323.15 K deviate from experimental measurements by between 20% at $p \lesssim 10$ MPa and 30% at $p \gtrsim 30$ MPa. In contrast, an agreement between 5 and 10% is observed between simulations and most experiments at 423.15 K and for all salt concentrations. Previous simulation studies by Liu et al.^{60,61} and Orozco et al.⁶² report similar disagreements between experiments and MC simulations at low temperatures. The culprit behind the discrepancies between simulations and experiments could either be the incorrect mixing rules describing the molecular interactions between CO_2 and H_2O , or the inaccuracies in the force fields developed for H_2O and CO_2 with respect to the solubility calculations.

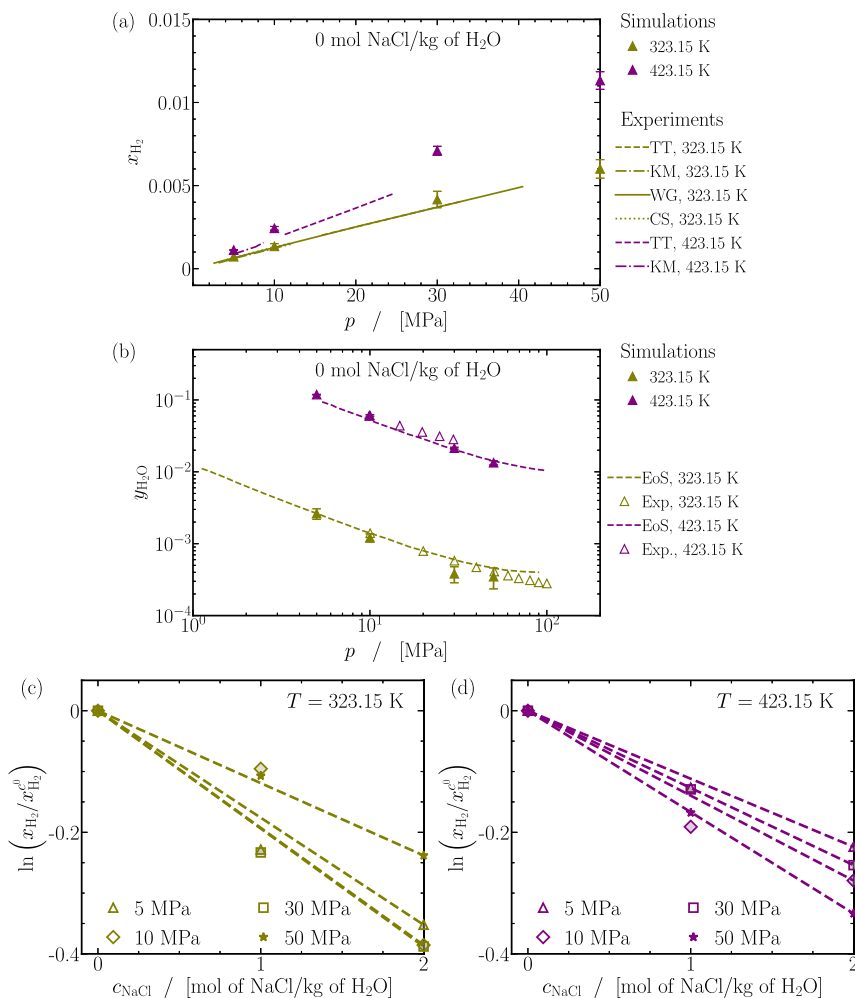


Figure 10. (a) Comparison of simulations (symbols) with experimental (lines) predictions for H₂ solubilities in pure H₂O. Experimental studies of Torín Ollarves and Trusler (TT),⁷⁹ Kling and Maurer (KM),¹⁷² Wiebe and Gaddy (WG),¹⁷³ and Chabab et al. (SC)⁵⁷ are considered for the comparison. (b) Comparison of the water content in the gas phase between our simulations and the experiments from Torín Ollarves and Trusler (TT). Predictions from the equation of state from Torín Ollarves and Trusler (TT) are also plotted alongside. (c,d) Reduction in the solubility of H₂ as a function of NaCl concentration in brine. The logarithm of the ratio of H₂ solubility in brine to its solubility in pure water is plotted against NaCl concentration. Linear fits to the data are shown as dashed lines. The raw data of the solubilities are provided in Table S5 of the Supporting Information.

The salting-out effect occurs in solutions when certain salts (ionic compounds) are added, leading to a decrease in the solubility of nonionic solutes in the solvent, typically organic compounds. This is due to the presence of ions in the solution altering the interactions between solvent and solute molecules, resulting in reduced solubility.¹³⁹ The salting-out effect has been well studied in the context of CO₂ solubility in aqueous solutions of many ionic salts, including NaCl.^{55,56,88} The influence of salt concentration on the solubility of CO₂ becomes evident when plotting the ratio of x_{CO_2} relative to its solubility in pure water under the same thermodynamic conditions, as a function of the salt concentration. This is the well-known Setschenow equation¹⁴⁰

$$\ln \left(\frac{x_{\text{CO}_2}}{x_{\text{CO}_2}^0} \right) = K c_{\text{NaCl}} \quad (12)$$

where $x_{\text{CO}_2}^0$ is the reference solubility of CO₂ in H₂O at the same pressure at a chosen temperature. In Figure 9d,e, the solubility ratios are plotted on the vertical axis as a function of

the salt concentration, in a format consistent with the Setschenow equation (eq 12). A linear relationship is observed between the solubility ratios and salt concentration, consistent with eq 12, exhibiting a slope of ca. -0.21 regardless of temperature and pressure. The negative slope implies a reduced solubility of CO₂ in brine upon increasing the salt concentration. Specifically, the solubility of CO₂ reduces, at any chosen pressure and temperature, by ca. 20% when a mole of NaCl is added to pure water results. A subsequent rise in salt concentration to 2 mol NaCl/kg H₂O results in a further reduction of CO₂ by another ca. 20%.

As an additional check of our simulations, the fugacity coefficients of CO₂ in the gas phase computed along the VLE of CO₂-NaCl brine at a given composition (y_{CO_2} , $y_{\text{H}_2\text{O}}$), pressure, and temperature are compared to the data from REFPROP.¹⁰⁸ Fugacity coefficients are a direct reflection of the excess chemical and mixture density, as indicated by eq 6. In general, the values of φ_{CO_2} and $\varphi_{\text{H}_2\text{O}}$ were below unity, signifying the nonideality of CO₂-H₂O mixtures in the gas phase. The fugacity coefficients were found to decrease with

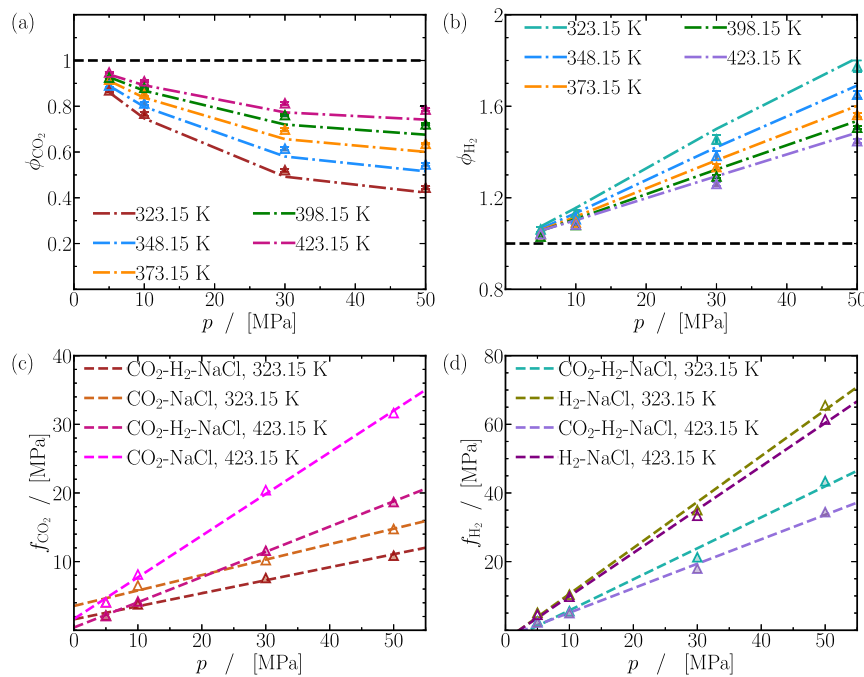


Figure 11. Fugacity coefficients and fugacities of CO₂ and H₂ in the CO₂-H₂-NaCl brine system computed from MC simulations using eq 6. Fugacity coefficients of (a) CO₂ and (b) H₂ in the gas-rich phase compared to predictions from REFPROP¹⁰⁸ based on the gas-phase compositions from MC simulations depicted by dashed lines. (c,d) Fugacities of CO₂ and H₂ computed from eq 13 using fugacity coefficients from (a,b), respectively. The dashed lines are linear fits to the data points. The open symbols represent fugacities computed for CO₂ and H₂ in the respective binary systems of CO₂-NaCl and H₂-NaCl, respectively. The raw data of the fugacity coefficients are provided in Table S7 of the Supporting Information.

pressure and increase with temperature. For all thermodynamic conditions investigated in our study, the values of φ_{CO_2} and $\varphi_{\text{H}_2\text{O}}$ agreed with REFPROP¹⁰⁸ within 2–3%.

The water content in the gas phase $y_{\text{H}_2\text{O}}$ at 323.15 and 423.15 K is plotted in Figure 12e,f. Clearly, from Figure 12e,f, a substantial quantity of water is present in the gas phase at 423.15 K in comparison to 323.15 K. At 323.15 K, the water content in the gas phase is unaffected by pressure, while the water content decreases by ca. 3 times between 5 and 50 MPa at 423.15 K. The quantity of water in the gas phase is insensitive to the NaCl concentration in brine.

Additional plots pertaining to the effect of temperature, pressure, and salt concentration on the VLE CO₂-NaCl brine systems is shown in Figures S35–S37 of the Supporting Information.

3.7. Phase Equilibria of H₂-NaCl Brine Mixtures. Figure 10a shows the solubilities of H₂ in pure water at 323.15 and 423.15 K for pressures between 5 and 50 MPa. In Figure 10a, the H₂ solubility in pure H₂O shows a linear increase with pressure, indicating adherence to the Henry regime across the pressure range, with solubilities approaching 0 in the limit of $p \rightarrow 0$. Increasing the pressure from 5 to 50 MPa leads to a near-10-fold increase in the solubility of H₂. Interestingly, the impact of pressure on H₂ solubility remains consistent regardless of salt concentration or temperature. In contrast to CO₂, increasing temperature consistently enhances the dissolution of H₂ in both H₂O and NaCl brine. The impact of temperature however is less pronounced in NaCl brine, where a smaller increase in solubility is observed compared to pure H₂O. For instance, an increase in temperature from 323.15 to 423.15 K results in a ca. 80% increase in solubility in pure H₂O, whereas the increase is around 40% in brine containing 1 mol NaCl/kg of H₂O, and nearly 30% in brine containing 2 mol NaCl/kg of H₂O.

The solubilities of H₂ in NaCl brine computed from MC simulations are compared to the available literature data in Figure 10a. Computed solubilities agree within ca. 5–10% of the experimental data from Torín-Ollarves and Trusler⁷⁹ for the entire range of pressures at 323.15 K. Disagreements between simulations and experiments arise at 423.15 K, with the solubilities being overestimated by simulations by a maximum of ca. 27% at $p = 30$ MPa. In Figure 10a, the disagreement between simulations and experiments at 423.15 K increases with pressure. The water content in the gas phase ($y_{\text{H}_2\text{O}}$) shown in Figure 10b at 323.15 and 423.15 K aligns well with the experimental data from Torín-Ollarves and Trusler,⁷⁹ with deviations between 5 and 10% for various pressures.

The salting-out effect in H₂ solubility on NaCl brine has been explored in experiments by Chabab et al.^{57,59} Plotting the solubility ratios as a function of the salt concentration according to the Setschenow equation (eq 12) yields a linear relation, as shown in Figure 10c,d. Unlike CO₂ in Figure 9d,e, the fitted lines have different slopes, suggesting a minor sensitivity of the salting-out effect on the pressure. The slopes of the fitted lines in Figure 10c,d fall between [−0.11, −0.19]. The solubility of H₂ reduces, at any chosen pressure and temperature, by ca. 15% when a mole of NaCl is added to pure water results. A subsequent rise in salt concentration to 2 mol NaCl/kg H₂O results in a further reduction of CO₂ by another ca. 15%.

The mole fraction of water in the gas phase ($y_{\text{H}_2\text{O}}$) at 323.15 and 423.15 K is plotted in Figure 12e,f. Figure 12e,f clearly shows that the water content in the gas phase at 423.15 K can be 20 to 40 times higher compared to 323.15 K. Similar to the

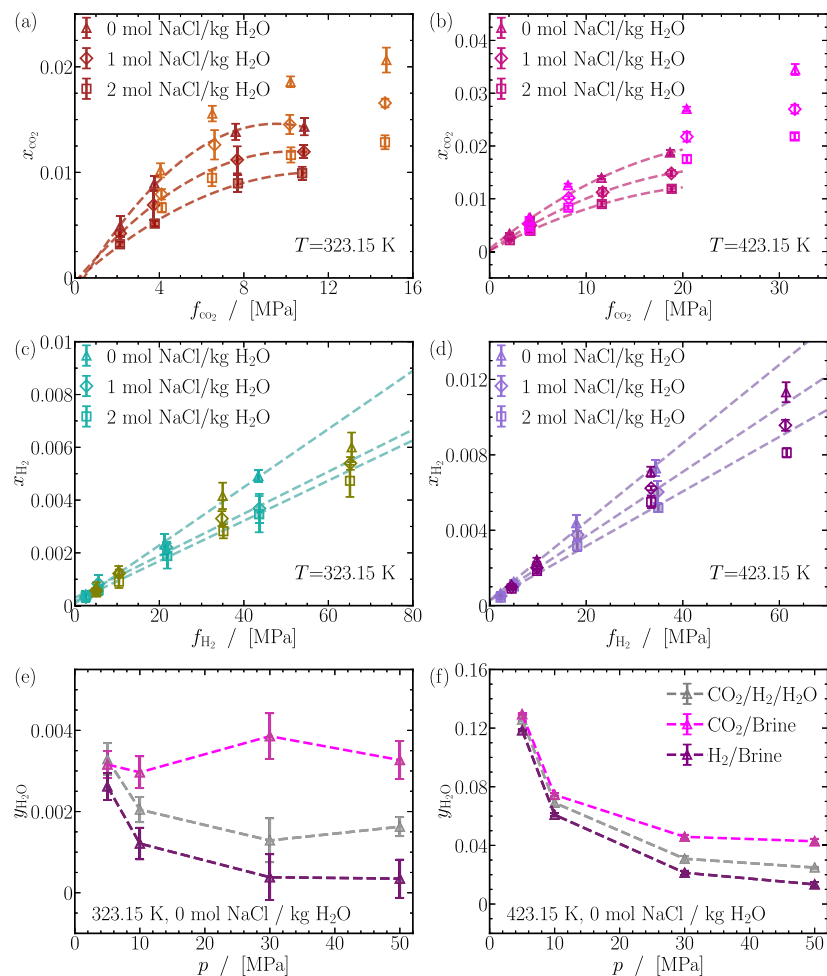


Figure 12. Mole fractions of CO_2 (x_{CO_2}) and H_2 (x_{H_2}) in the liquid-rich phase are presented for the $\text{H}_2\text{-CO}_2\text{-NaCl}$ system (closed symbols) and compared with the $\text{CO}_2\text{-NaCl}$ and $\text{H}_2\text{-NaCl}$ systems (open symbols). (a,b) x_{CO_2} as a function of the fugacity of CO_2 in the gas-rich phase at 323.15 and 423.15 K, respectively. Quadratic fits for x_{CO_2} in the $\text{H}_2\text{-CO}_2\text{-NaCl}$ system are represented by dashed lines. (c,d) serve the same purpose for H_2 . (e,f) Comparison of the water content in the $\text{CO}_2\text{-H}_2\text{-H}_2\text{O}$ (ternary) system with the $\text{CO}_2\text{-H}_2\text{O}$ and $\text{H}_2\text{-H}_2\text{O}$ (binary) systems at 323.15 and 423.15 K. The raw data of the solubilities are provided in Table S6 of the Supporting Information.

$\text{CO}_2\text{-NaCl}$ brine system, the salt concentration in brine appears to have little or negligible effect on the quantity of water in the gas phase. Figure 12e,f also show that the water content in the gas-rich phase decreases with pressure. The fugacity coefficients of H_2 and H_2O obtained from MC simulations (eq 6) closely align with REFPROP predictions, showing agreement within a 5% margin for identical $\text{H}_2\text{-H}_2\text{O}$ mixtures at various compositions, pressures, and temperatures. Notably, ϕ_{H_2} consistently surpasses unity, indicating prevalent repulsive interactions among H_2 molecules in the gas phase. This contrasts with the fugacity coefficients for CO_2 in $\text{CO}_2\text{-NaCl}$ brine systems, which are below 1, suggesting attractive interactions between CO_2 molecules in the gas phase. Additional plots pertaining to the effect of temperature, pressure, and salt concentration on the VLE $\text{H}_2\text{-NaCl}$ brine systems is shown in Figures S35–S37 of the Supporting Information.

3.8. Phase Equilibria of $\text{CO}_2\text{-H}_2\text{-NaCl}$ Brine Mixtures. The phase equilibria of $\text{H}_2\text{-CO}_2\text{-NaCl}$ brine systems are investigated to compare the solubilities of CO_2 and H_2 in pure water and NaCl brine with their solubilities in binary systems: $\text{CO}_2\text{-NaCl}$ brine and $\text{H}_2\text{-NaCl}$. The dissolution of CO_2 and H_2

in NaCl brine is examined as a function of fugacity rather than pressure, as fugacity serves as a measure of the chemical potential responsible for gas dissolution in water. The fugacity of component i (f_i), where i is either CO_2 or H_2 , is^{52,53}

$$f_i = \phi_i(p, T, y_i) y_i p \quad (13)$$

where ϕ_i is the fugacity coefficient, as defined in eq 6, y_i is the mole fraction of species i in the gas phase, and p is the pressure.

The fugacity coefficients and the fugacities of CO_2 and H_2 are shown in Figure 11a–d as a function of pressure between 323.15 and 423.15 K along the VLE of $\text{CO}_2\text{-H}_2\text{-NaCl}$ brine. In Figure 11a, the fugacity coefficients of CO_2 behave similarly to those in the $\text{CO}_2\text{-NaCl}$ brine system. Specifically, ϕ_{CO_2} decreases with pressure but increases with temperature. Computed fugacity coefficients derived from gas phase compositions along the VLE of $\text{CO}_2\text{-H}_2\text{-NaCl}$ brine agree within ca. 5–10% of the REFPROP predictions. In Figure 11c, fugacities of CO_2 computed using eq 13 vary linearly with pressure, as indicated by the fits at 323.15 and 423.15 K. Unlike CO_2 , the fugacity coefficients of H_2 shown in Figure 11b exhibit an increase with pressure but a decrease with

temperature, qualitatively reproducing its behavior in the binary mixture of H₂-NaCl brine. Fugacities of H₂ computed using eq 13 vary linearly with pressure, as indicated by the fits at 323.15 and 423.15 K in Figure 11d. To facilitate comparison, open symbols representing the fugacities of CO₂ and H₂ in the binary systems of CO₂-NaCl and H₂-NaCl are plotted alongside the ternary system in Figure 11c,d. The fugacities of CO₂ and H₂ in the ternary CO₂-H₂-NaCl systems are lower than those in their respective binary systems. For instance, in Figure 11c, the fugacity of CO₂ in the ternary system at 50 MPa and 423.15 K is lower by ca. 45% than f_{CO_2} in the binary system. Similarly, in the case of H₂ in Figure 11d, the fugacities in the ternary system are lower by ca. 40% at 50 MPa and 423.15 K.

The solubilities of CO₂ and H₂ in NaCl brine solutions are shown in Figure 12a-d, comparing binary and ternary systems. The solubility of CO₂ varies quadratically with the fugacity of CO₂ in both binary and ternary systems, as shown in Figure 12a. In the low-fugacity regime ($f_{\text{CO}_2} \lesssim 4$ MPa), the solubilities of CO₂ in NaCl brine are similar for the binary and ternary systems. For intermediate and large fugacities ($f_{\text{CO}_2} \gtrsim 4$ MPa), the solubility of CO₂ in NaCl brine becomes substantially different in the binary and ternary systems. Specifically, CO₂ solubility in the ternary system is lower compared to the binary system at (approximately) the same fugacity. An even stronger suppression in the dissolution of CO₂ occurs at 423.15 K, as shown in Figure 12b. The solubilities of H₂ in NaCl brine shown in Figure 12c,d is analyzed next. In the low-fugacity regime ($f_{\text{H}_2} \lesssim 40$ MPa), the solubilities of H₂ are nearly identical in the binary and ternary systems. Differences in the solubilities arise for $f_{\text{H}_2} \gtrsim 40$, wherein a greater H₂ dissolution is evident in the ternary case when compared to the H₂-NaCl brine system. The enhanced dissolution occurs also at 423.15 K, as shown in Figure 12d. In contrast to CO₂, the solubility of H₂ as a function of f_{H_2} is enhanced in ternary systems.

Figure 12e,f show the water content in the gas phase for both binary and ternary systems. The water content in the gas phase varies negligibly with the salt concentration in brine. In Figure 12e at 323.15 K, the mole fraction of H₂O in the gas phase decreases with pressure for CO₂-H₂-H₂O systems. As expected, the mole fraction of water in the ternary system falls between those of the CO₂-H₂O and H₂-H₂O binary systems. At 423.15 K, the water content in the gas phase is higher, yet it follows a trend similar to that at 323.15 K. In conclusion, an enhanced dissolution of water is observed compared to the H₂-brine system but suppression compared to the CO₂-brine system.

4. CONCLUSIONS

Understanding the thermodynamic behavior of mixtures containing H₂ and CO₂ is essential for addressing hydrogen losses in underground hydrogen storage within depleted gas fields. The loss of purity of H₂ resulting from molecular diffusion follows Fick's law, highlighting the importance of knowing the Fick diffusion coefficients for a variety of temperatures, pressures, and mixture compositions. The dissolution of H₂ in salt water, particularly in the presence of CO₂, presents another avenue for hydrogen loss. Thus, a comprehensive knowledge of the Fick diffusion coefficients for H₂-CO₂ mixtures and their phase equilibria with NaCl brine is

crucial. The thermodynamic conditions relevant to subsurface hydrogen storage typically span temperatures of 323.15 to 423.15 K, pressures ranging from 5 to 50 MPa, and salt concentrations of 1 to 2 mol of NaCl/kg of H₂O.

The Fick diffusivities of H₂-CO₂ mixtures were investigated via MD simulations at storage-relevant conditions. At low pressures (5 MPa), gas-like diffusivities of ca. 10⁻⁶ m²/s remained composition-independent. The kinetic theory accurately predicted these diffusivities within 5–10% at 423.15 K, with deviations of up to 20% at 323.15 K. At high pressures (40–50 MPa), kinetic theory predictions deviated up to 75% for CO₂-rich mixtures and around 15% for hydrogen-enriched ones. Approaches based on kinetic theory, such as the Fuller correlation^{30–32} and the corresponding-states approaches,^{11,13} yielded similar results. Kinetic theory-based methods can predict Fick diffusivities within 15% for H₂-CO₂ mixtures exhibiting near-ideal gas behavior (1) at low pressures (ca. 5 MPa) and high temperatures (423.15 K) and (2) for H₂-enriched mixtures (mole fraction of H₂ $\gtrsim 0.8$). Moggridge correlation^{122,130–134} provides an alternative to accurately predicting diffusion coefficients within 5–10% at high pressures (40–50 MPa) and low temperatures ($T \lesssim 348.15$ K) for CO₂-rich mixtures, making it suitable for the high-pressure regime. For intermediate pressures (10–35 MPa), molecular simulations are preferred. The efficacy of the Moggridge correlation stems from the fluid-like behavior of mixtures at high pressures. Mixtures at 323.15 K and pressures of 15–25 MPa exhibit oscillatory trends in Fick diffusivities due to the proximity of CO₂ to its critical point.

Phase equilibria of CO₂-H₂-NaCl mixtures are examined using CFCMC simulations showing close agreement with experimental results for CO₂ solubilities in NaCl brines. The Setschenow equation¹⁴⁰ used to describe the salting-out effect of CO₂ captures the exponentially decreasing solubilities of CO₂ in the liquid-rich phase with an increasing concentration of NaCl in brine. The water content in the gas phase decreased with pressure at 423.15 K but remained nearly constant at 323.15 K, regardless of salt concentration. H₂ solubilities in brine followed the Henry regime, varying linearly with pressure. The impact of salt concentration on H₂ solubility relative to pure water is quantified using the Setschenow equation. Similar to the CO₂-NaCl brine system, water concentrations in the gas phase consistently decrease with pressure at both 323.15 and 423.15 K. Ternary systems of H₂-CO₂-NaCl brine mixtures revealed a suppressed CO₂ solubility and an enhanced H₂ solubility, compared to the solubilities in the respective binary mixtures. The water content in the gas phase is enhanced compared to H₂-NaCl brine systems but suppressed compared to CO₂-NaCl brine systems.

■ ASSOCIATED CONTENT

SI Supporting Information

The Supporting Information is available free of charge at <https://pubs.acs.org/doi/10.1021/acs.iecr.4c01078>.

Mixture densities, mixture compressibility factors, mixture viscosities, self-diffusion coefficients, finite system-size effects on self-diffusion coefficients, self-diffusivities, ratio of self-diffusion coefficients, ratio of self-diffusivities, effect of temperature on self-diffusion coefficients, density dependence of self-diffusion coefficients, Maxwell-Stefan diffusion coefficients from cross-correlations of displacements, finite-size effects for the

mutual diffusion coefficients, Fick diffusion coefficients, effect of mixture composition and temperature on Fick diffusion coefficients, principle of corresponding states for Fick diffusivities, effect of pressure, temperature, and NaCl concentration on the solubility, force field parameters, densities, compressibilities, and total energies from MD simulations, viscosities, thermodynamic factors, and self, Maxwell-Stefan, and Fick diffusion coefficients, phase equilibria, and fugacity coefficients ([PDF](#))

AUTHOR INFORMATION

Corresponding Author

Thijs J. H. Vlugt — *Engineering Thermodynamics, Process and Energy Department, Faculty of Mechanical Engineering, Delft University of Technology, Delft 2628 CB, The Netherlands;* orcid.org/0000-0003-3059-8712; Email: t.j.h.vlugt@tudelft.nl

Authors

Thejas Hulikal Chakrapani — *Reservoir Engineering, Geoscience and Engineering Department, Faculty of Civil Engineering and Geosciences, Delft University of Technology, Delft 2628 CN, The Netherlands;* orcid.org/0000-0002-8182-345X

Hadi Hajibeygi — *Reservoir Engineering, Geoscience and Engineering Department, Faculty of Civil Engineering and Geosciences, Delft University of Technology, Delft 2628 CN, The Netherlands*

Othonas A. Moultos — *Engineering Thermodynamics, Process and Energy Department, Faculty of Mechanical Engineering, Delft University of Technology, Delft 2628 CB, The Netherlands;* orcid.org/0000-0001-7477-9684

Complete contact information is available at:

<https://pubs.acs.org/10.1021/acs.iecr.4c01078>

Notes

The authors declare no competing financial interest.

ACKNOWLEDGMENTS

H.H. and T.H.C. are sponsored by the Dutch National Science Foundation (NWO) Talent Programme ViDi Project “ADMIRE” (grant number 17509). This work was also sponsored by NWO Domain Science for the use of supercomputer facilities. The authors acknowledge the use of the computational resources of the DelftBlue supercomputer, provided by the Delft High Performance Computing Centre (<https://www.tudelft.nl/dhpc>). T.H.C. acknowledges the use of the computing cluster at the Civil Engineering Department at Delft University of Technology.

REFERENCES

- (1) Hassanpouryouzband, A.; Joonaki, E.; Edlmann, K.; Haszeldine, R. S. Offshore geological storage of hydrogen: is this our best option to achieve net-zero? *ACS Energy Lett.* **2021**, *6*, 2181–2186.
- (2) Heinemann, N.; Alcalde, J.; Miocic, J. M.; Hangx, S. J. T.; Kallmeyer, J.; Ostertag-Henning, C.; Hassanpouryouzband, A.; Thayesen, E. M.; Strobel, G. J.; Schmidt-Hattenberger, C.; Edlmann, K.; Wilkinson, M.; Bentham, M.; Stuart Haszeldine, R.; Carbonell, R.; Rudloff, A. Enabling large-scale hydrogen storage in porous media – the scientific challenges. *Energy Environ. Sci.* **2021**, *14*, 853–864.
- (3) Hematpur, H.; Abdollahi, R.; Rostami, S.; Haghghi, M.; Blunt, M. J. Review of Underground Hydrogen Storage: Concepts and challenges. *Adv. Geo-Energy Res.* **2023**, *7*, 111–131.
- (4) Krevor, S.; De Coninck, H.; Gasda, S. E.; Ghaleigh, N. S.; de Gooyer, V.; Hajibeygi, H.; Juanes, R.; Neufeld, J.; Roberts, J. J.; Swennenhuis, F. Subsurface carbon dioxide and hydrogen storage for a sustainable energy future. *Nat. Rev. Earth Environ.* **2023**, *4*, 102–118.
- (5) Lehtola, T.; Zahedi, A. Solar energy and wind power supply supported by storage technology: A review. *Sustain. Energy Technol. Assess.* **2019**, *35*, 25–31.
- (6) Tarkowski, R. Underground hydrogen storage: Characteristics and prospects. *Renewable Sustainable Energy Rev.* **2019**, *105*, 86–94.
- (7) Oldenburg, C. M. Carbon Dioxide as Cushion Gas for Natural Gas Storage. *Energy Fuels* **2003**, *17*, 240–246.
- (8) Oldenburg, C. M.; Pan, L. Utilization of CO₂ as cushion gas for porous media compressed air energy storage. *Greenhouse Gases: Sci. Technol.* **2013**, *3*, 124–135.
- (9) Fick, A. Ueber Diffusion. *Ann. Phys.* **1855**, *170* (1), 59–86.
- (10) Taylor, R.; Krishna, R. *Multicomponent Mass Transfer*, 1st ed.; John Wiley & Sons: New York, 1993.
- (11) Cussler, E. L. *Diffusion: Mass Transfer in Fluid Systems*, 3rd ed.; Cambridge University press: Cambridge, 2009.
- (12) Krishna, R.; Wesselingh, J. A. The Maxwell-Stefan Approach to Mass Transfer. *Chem. Eng. Sci.* **1997**, *52*, 861–911.
- (13) Poling, B. E.; Prausnitz, J. M.; O’Connel, J. P. *Properties of Gases and Liquids*, 5th ed.; McGraw-Hill Education: New York, 2001.
- (14) Dorfman, J. R.; van Beijeren, H.; Kirkpatrick, T. R. *Contemporary Kinetic Theory of Matter*, 1st ed.; Cambridge University Press, 2021.
- (15) Liu, X.; Bardow, A.; Vlugt, T. J. H. Multicomponent Maxwell-Stefan Diffusivities at Infinite Dilution. *Ind. Eng. Chem. Res.* **2011**, *50*, 4776–4782.
- (16) Enskog, D. Kinetic theory of heat conductivity, viscosity and diffusion in certain condensed gases and liquids. *Kungl. Svenska Vetenskap. Handl.* **1922**, *63*, 1–44.
- (17) Hirschfelder, J. O.; Curtiss, C. F.; Bird, R. B. *The Molecular Theory of Gases and Liquids*, 1st ed.; John Wiley & Sons: New York, 1954.
- (18) Chapman, S.; Cowling, T. G. *The Mathematical Theory of Non-uniform Gases: An Account of the Kinetic Theory of Viscosity, Thermal Conduction and Diffusion in Gases*, 3rd ed.; Cambridge University Press: Cambridge, 1970.
- (19) Marrero, T. R.; Mason, E. A. Gaseous Diffusion Coefficients. *J. Phys. Chem. Ref. Data* **1972**, *1*, 3–118.
- (20) Sharipov, F.; Benites, V. J. Transport coefficients of argon and its mixtures with helium and neon at low density based ab initio potentials. *Fluid Phase Equilib.* **2019**, *498*, 23–32.
- (21) Hellmann, R. Cross Second Virial Coefficients and Dilute Gas Transport Properties of the Systems (N₂ + C₃H₈), (C₂H₆ + C₃H₈), and (H₂S + C₃H₈) from Ab Initio-Based Intermolecular Potentials. *J. Chem. Eng. Data* **2020**, *65*, 4712–4724.
- (22) Van Beijeren, H.; Ernst, M. The non-linear Enskog-Boltzmann equation. *Phys. Lett. A* **1973**, *43*, 367–368.
- (23) Jervell, V. G.; Wilhelmsen, Ø. Revised Enskog theory for Mie fluids: Prediction of diffusion coefficients, thermal diffusion coefficients, viscosities, and thermal conductivities. *J. Chem. Phys.* **2023**, *158*, 224101.
- (24) Dunlop, P. J.; Robjohns, H. L.; Bignell, C. M. Diffusion and thermal diffusion in binary mixtures of hydrogen with noble gases. *J. Chem. Phys.* **1987**, *86*, 2922–2926.
- (25) Hogervorst, W. Diffusion coefficients of noble-gas mixtures between 300 K and 1400 K. *Physica* **1971**, *51*, 59–76.
- (26) Guevara-Carrion, G.; Anchirbak, S.; Mialdun, A.; Vrabec, J.; Shevtsova, V. Diffusion of methane in supercritical carbon dioxide across the Widom line. *Sci. Rep.* **2019**, *9*, 8466.
- (27) Li, H.; Wilhelmsen, Ø.; Lv, Y.; Wang, W.; Yan, J. Viscosities, thermal conductivities and diffusion coefficients of CO₂ mixtures:

- Review of experimental data and theoretical models. *Int. J. Greenhouse Gas Control* **2011**, *5*, 1119–1139.
- (28) Chou, C.-H.; Martin, J. J. Diffusion of Gases at Elevated Pressures—Carbon-14—Labeled CO₂ in CO₂—H₂ and CO₂—Propane. *Ind. Eng. Chem.* **1957**, *49*, 758–762.
- (29) Wilke, C. R.; Chang, P. Correlation of Diffusion Coefficients in Dilute Solutions. *AICHE J.* **1955**, *1*, 264–270.
- (30) Fuller, E. N.; Giddings, J. C. A comparison of methods for predicting gaseous diffusion coefficients. *J. Chromatogr. Sci.* **1965**, *3*, 222–227.
- (31) Fuller, E. N.; Schettler, P. D.; Giddings, J. C. A New Method for Prediction of Binary Gas-Phase Diffusion Coefficients. *Ind. Eng. Chem.* **1966**, *58*, 18–27.
- (32) Fuller, E. N.; Ensley, K.; Giddings, J. C. Diffusion of halogenated hydrocarbons in helium. The effect of structure on collision cross sections. *J. Phys. Chem.* **1969**, *73*, 3679–3685.
- (33) Takahashi, S.; Hongo, M. Diffusion coefficients of gases at high pressures in the CO₂-C₂H₄ system. *J. Chem. Eng. Jpn.* **1982**, *15*, 57–59.
- (34) Riazi, M. R.; Whitson, C. H. Estimating diffusion coefficients of dense fluids. *Ind. Eng. Chem. Res.* **1993**, *32*, 3081–3088.
- (35) Allen, M. P.; Tildesley, D. *Computer Simulation of Liquids*, 2nd ed.; Oxford University Press: Oxford, 2017.
- (36) Frenkel, D.; Smit, B. *Understanding Molecular Simulation. From Algorithms to Applications*, 3rd ed.; Elsevier Science: Oxford, 2023.
- (37) Tsimpanogiannis, I. N.; Jamali, S. H.; Economou, I. G.; Vlugt, T. J. H.; Mourtos, O. A. On the validity of the Stokes–Einstein relation for various water force fields. *Mol. Phys.* **2020**, *118*, No. e1702729.
- (38) Mourtos, O. A.; Tsimpanogiannis, I. N. Predictive model for the intra-diffusion coefficients of H₂ and O₂ in vapour H₂O based on data from molecular dynamics simulations. *Mol. Phys.* **2023**, *121*, No. e2211889.
- (39) Tsimpanogiannis, I. N.; Mourtos, O. A. Is Stokes–Einstein relation valid for the description of intra-diffusivity of hydrogen and oxygen in liquid water? *Fluid Phase Equilib.* **2023**, *563*, 113568.
- (40) Liu, X.; Schnell, S. K.; Simon, J.-M.; Bedeaux, D.; Kjelstrup, S.; Bardow, A.; Vlugt, T. J. H. Fick Diffusion Coefficients of Liquid Mixtures Directly Obtained from Equilibrium Molecular Dynamics. *J. Phys. Chem. B* **2011**, *115*, 12921–12929.
- (41) Liu, X.; Martín-Calvo, A.; McGarrity, E.; Schnell, S. K.; Calero, S.; Simon, J.-M.; Bedeaux, D.; Kjelstrup, S.; Bardow, A.; Vlugt, T. J. H. Fick Diffusion Coefficients in Ternary Liquid Systems from Equilibrium Molecular Dynamics Simulations. *Ind. Eng. Chem. Res.* **2012**, *51*, 10247–10258.
- (42) Liu, X.; Schnell, S. K.; Simon, J.-M.; Krüger, P.; Bedeaux, D.; Kjelstrup, S.; Bardow, A.; Vlugt, T. J. H. Diffusion Coefficients from Molecular Dynamics Simulations in Binary and Ternary Mixtures. *Int. J. Thermophys.* **2013**, *34*, 1169–1196.
- (43) Vella, J. R. Fick Diffusion Coefficients of the Gaseous CH₄–CO₂ System from Molecular Dynamics Simulations Using TraPPE Force Fields at 101.325, 506.625, 1013.25, 2533.12, and 5066.25 kPa. *J. Chem. Eng. Data* **2019**, *64*, 3672–3681.
- (44) Saric, D.; Guevara-Carrion, G.; Vrabec, J. Thermodynamics of supercritical carbon dioxide mixtures across the Widom line. *Phys. Chem. Chem. Phys.* **2022**, *24*, 28257–28270.
- (45) Saric, D.; Guevara-Carrion, G.; Gaponenko, Y.; Shevtsova, V.; Vrabec, J. Diffusion of hydrocarbons diluted in supercritical carbon dioxide. *Sci. Rep.* **2023**, *13*, 16107.
- (46) Rosenfeld, Y. Relation between the transport coefficients and the internal entropy of simple systems. *Phys. Rev. A* **1977**, *15*, 2545–2549.
- (47) Hopp, M.; Mele, J.; Gross, J. Self-diffusion coefficients from entropy scaling using the PCP-SAFT equation of state. *Ind. Eng. Chem. Res.* **2018**, *57*, 12942–12950.
- (48) Dyre, J. C. Perspective: Excess-entropy scaling. *J. Chem. Phys.* **2018**, *149*, 210901.
- (49) Bell, I. H.; Messerly, R.; Thol, M.; Costigliola, L.; Dyre, J. C. Modified entropy scaling of the transport properties of the Lennard-Jones fluid. *J. Phys. Chem. B* **2019**, *123*, 6345–6363.
- (50) Bell, I. H.; Dyre, J. C.; Ingebrigtsen, T. S. Excess-entropy scaling in supercooled binary mixtures. *Nat. Commun.* **2020**, *11*, 4300.
- (51) Ghaffarizadeh, S. A.; Wang, G. J. Excess Entropy Scaling in Active-Matter Systems. *J. Phys. Chem. Lett.* **2022**, *13*, 4949–4954.
- (52) Smith, J. M.; Van Ness, H. C.; Abbott, M. M.; Swihart, M. T. *Introduction to Chemical Engineering Thermodynamics*; McGraw-Hill: Singapore, 1949.
- (53) Sandler, S. *Chemical, Biochemical, and Engineering Thermodynamics*, 4th ed.; John Wiley & Sons: Hoboken, NJ, USA, 2006.
- (54) Spycher, N.; Pruess, K.; Ennis-King, J. CO₂-H₂O mixtures in the geological sequestration of CO₂. I. Assessment and calculation of mutual solubilities from 12 to 100 °C and up to 600 bar. *Geochim. Cosmochim. Acta* **2003**, *67*, 3015–3031.
- (55) Spycher, N.; Pruess, K. CO₂-H₂O mixtures in the geological sequestration of CO₂. II. Partitioning in chloride brines at 12–100 °C and up to 600 bar. *Geochim. Cosmochim. Acta* **2005**, *69*, 3309–3320.
- (56) Duan, Z.; Sun, R. An improved model calculating CO₂ solubility in pure water and aqueous NaCl solutions from 273 to 533 K and from 0 to 2000 bar. *Chem. Geol.* **2003**, *193*, 257–271.
- (57) Chabab, S.; Theveneau, P.; Coquelet, C.; Corvisier, J.; Paricaud, P. Measurements and predictive models of high-pressure H₂ solubility in brine (H₂O + NaCl) for underground hydrogen storage application. *Int. J. Hydrogen Energy* **2020**, *45*, 32206–32220.
- (58) Ansari, S.; Safaei-Farouji, M.; Atashrouz, S.; Abedi, A.; Hemmati-Sarapardeh, A.; Mohaddespour, A. Prediction of hydrogen solubility in aqueous solutions: Comparison of equations of state and advanced machine learning-metaheuristic approaches. *Int. J. Hydrogen Energy* **2022**, *47*, 37724–37741.
- (59) Chabab, S.; Kerkache, H.; Bouchkira, I.; Poulain, M.; Baudouin, O.; Moine, E.; Ducoussو, M.; Hoang, H.; Galliéro, G.; Cézac, P. Solubility of H₂ in water and NaCl brine under subsurface storage conditions: Measurements and thermodynamic modeling. *Int. J. Hydrogen Energy* **2024**, *50*, 648–658.
- (60) Liu, Y.; Panagiotopoulos, A. Z.; Debenedetti, P. G. Monte Carlo simulations of high-pressure phase equilibria of CO₂–H₂O mixtures. *J. Phys. Chem. B* **2011**, *115*, 6629–6635.
- (61) Liu, Y.; Lafitte, T.; Panagiotopoulos, A. Z.; Debenedetti, P. G. Simulations of vapor–liquid phase equilibrium and interfacial tension in the CO₂–H₂O–NaCl system. *AICHE J.* **2013**, *59*, 3514–3522.
- (62) Orozco, G. A.; Economou, I. G.; Panagiotopoulos, A. Z. Optimization of intermolecular potential parameters for the CO₂/H₂O mixture. *J. Phys. Chem. B* **2014**, *118*, 11504–11511.
- (63) Vorholz, J.; Harismiadis, V.; Rumpf, B.; Panagiotopoulos, A.; Maurer, G. Vapor+liquid equilibrium of water, carbon dioxide, and the binary system, water+carbon dioxide, from molecular simulation. *Fluid Phase Equilib.* **2000**, *170*, 203–234.
- (64) Lobanova, O.; Mejía, A.; Jackson, G.; Müller, E. A. SAFT- γ force field for the simulation of molecular fluids 6: Binary and ternary mixtures comprising water, carbon dioxide, and n-alkanes. *J. Chem. Thermodyn.* **2016**, *93*, 320–336.
- (65) Jiang, H.; Economou, I. G.; Panagiotopoulos, A. Z. Phase equilibria of water/CO₂ and water/n-alkane mixtures from polarizable models. *J. Phys. Chem. B* **2017**, *121*, 1386–1395.
- (66) Rahbari, A.; Brenkman, J.; Hens, R.; Ramdin, M.; van den Broeke, L. J. P.; Schoon, R.; Henkes, R.; Mourtos, O. A.; Vlugt, T. J. H. Solubility of Water in Hydrogen at High Pressures: A Molecular Simulation Study. *J. Chem. Eng. Data* **2019**, *64*, 4103–4115.
- (67) Rahbari, A.; Hens, R.; Dubbeldam, D.; Vlugt, T. J. H. Improving the accuracy of computing chemical potentials in CFCMC simulations. *Mol. Phys.* **2019**, *117*, 3493–3508.
- (68) Rumpf, B.; Nicolaisen, H.; Öcal, C.; Maurer, G. Solubility of carbon dioxide in aqueous solutions of sodium chloride: experimental results and correlation. *J. Solution Chem.* **1994**, *23*, 431–448.
- (69) Drummond, S. E., Jr. Boiling and mixing of hydrothermal fluids: chemical effects on mineral precipitation. Ph.D. Thesis, The Pennsylvania State University, 1981.

- (70) Malinin, S. D.; Saveleva, N. I. Experimental investigations of CO_2 solubility in NaCl and CaCl_2 solutions at temperatures of 25, 50 and 75 degrees and elevated CO_2 pressure. *Geokhim.* **1972**, *6*, 643.
- (71) Malinin, S.; Kurovskaya, N. Investigation of CO_2 solubility in a solution of chlorides at elevated temperatures and pressures of CO_2 . *Geokhim* **1975**, *4*, 547–551.
- (72) Nighswander, J. A.; Kalogerakis, N.; Mehrotra, A. K. Solubilities of carbon dioxide in water and 1 wt.% sodium chloride solution at pressures up to 10 MPa and temperatures from 80 to 200. degree. C. *J. Chem. Eng. Data* **1989**, *34*, 355–360.
- (73) Bando, S.; Takemura, F.; Nishio, M.; Hihara, E.; Akai, M. Solubility of CO_2 in aqueous solutions of NaCl at (30 to 60) °C and (10 to 20) MPa. *J. Chem. Eng. Data* **2003**, *48*, 576–579.
- (74) Kiepe, J.; Horstmann, S.; Fischer, K.; Gmehling, J. Experimental determination and prediction of gas solubility data for $\text{CO}_2 + \text{H}_2\text{O}$ mixtures containing NaCl or KCl at temperatures between 313 and 393 K and pressures up to 10 MPa. *Ind. Eng. Chem. Res.* **2002**, *41*, 4393–4398.
- (75) Spycher, N.; Pruess, K. A phase-partitioning model for CO_2 -brine mixtures at elevated temperatures and pressures: application to CO_2 -enhanced geothermal systems. *Transp. Porous Media* **2010**, *82*, 173–196.
- (76) Potoff, J. J.; Siepmann, J. I. Vapor-liquid Equilibria of Mixtures Containing Alkanes, Carbon Dioxide and Nitrogen. *AIChE J.* **2001**, *47*, 1676–1682.
- (77) Eggimann, B. L.; Sun, Y.; DeJaco, R. F.; Singh, R.; Ahsan, M.; Josephson, T. R.; Siepmann, J. I. Assessing the Quality of Molecular Simulations for Vapor–Liquid Equilibria: An Analysis of the TraPPE Database. *J. Chem. Eng. Data* **2020**, *65*, 1330–1344.
- (78) Abascal, J. L. F.; Vega, C. A general purpose model for the condensed phases of water: TIP4P/2005. *J. Chem. Phys.* **2005**, *123*, 234505.
- (79) Torín-Ollarves, G. A.; Trusler, J. M. Solubility of hydrogen in sodium chloride brine at high pressures. *Fluid Phase Equilib.* **2021**, *539*, 113025.
- (80) Chabab, S.; Théveneau, P.; Corvisier, J.; Coquelet, C.; Paricaud, P.; Houriez, C.; Ahmar, E. E. Thermodynamic study of the $\text{CO}_2-\text{H}_2\text{O}-\text{NaCl}$ system: Measurements of CO_2 solubility and modeling of phase equilibria using Soreide and Whitson, electrolyte CPA and SIT models. *Int. J. Greenhouse Gas Control* **2019**, *91*, 102825.
- (81) Peng, D.-Y.; Robinson, D. B. A new two-constant equation of state. *Ind. Eng. Chem. Res.* **1976**, *15*, 59–64.
- (82) Kontogeorgis, G. M.; Voutsas, E. C.; Yakoumis, I. V.; Tassios, D. P. An equation of state for associating fluids. *Ind. Eng. Chem. Res.* **1996**, *35*, 4310–4318.
- (83) Kontogeorgis, G. M.; Michelsen, M. L.; Folas, G. K.; Derawi, S.; Von Solms, N.; Stenby, E. H. Ten years with the CPA (Cubic-Plus-Association) equation of state. Part 1. Pure compounds and self-associating systems. *Ind. Eng. Chem. Res.* **2006**, *45*, 4855–4868.
- (84) Kontogeorgis, G. M.; Michelsen, M. L.; Folas, G. K.; Derawi, S.; Von Solms, N.; Stenby, E. H. Ten years with the CPA (Cubic-Plus-Association) equation of state. Part 2. Cross-associating and multicomponent systems. *Ind. Eng. Chem. Res.* **2006**, *45*, 4869–4878.
- (85) Krichevsky, I. R.; Kasarnovsky, J. S. Thermodynamical Calculations of Solubilities of Nitrogen and Hydrogen in Water at High Pressures. *J. Am. Chem. Soc.* **1935**, *57*, 2168–2171.
- (86) Chen, C.-C.; Britt, H. I.; Boston, J.; Evans, L. Local composition model for excess Gibbs energy of electrolyte systems. Part I: Single solvent, single completely dissociated electrolyte systems. *AIChE J.* **1982**, *28*, 588–596.
- (87) Chen, C.-C.; Evans, L. B. A local composition model for the excess Gibbs energy of aqueous electrolyte systems. *AIChE J.* **1986**, *32*, 444–454.
- (88) Duan, Z.; Sun, R.; Zhu, C.; Chou, I.-M. An improved model for the calculation of CO_2 solubility in aqueous solutions containing Na^+ , K^+ , Ca^{2+} , Mg^{2+} , Cl^- , and SO_4^{2-} . *Mar. Chem.* **2006**, *98*, 131–139.
- (89) Zhu, Z.; Cao, Y.; Zheng, Z.; Chen, D. An accurate model for estimating H_2 solubility in pure water and aqueous NaCl solutions. *Energies* **2022**, *15*, 5021.
- (90) Søreide, I.; Whitson, C. H. Peng-Robinson predictions for hydrocarbons, CO_2 , N_2 , and H_2S with pure water and NaCl brine. *Fluid Phase Equilib.* **1992**, *77*, 217–240.
- (91) Kerkache, H.; Hoang, H.; Cézac, P.; Galliéro, G.; Chabab, S. The solubility of H_2 in NaCl brine at high pressures and high temperatures: Molecular simulation study and thermodynamic modeling. *J. Mol. Liq.* **2024**, *400*, 124497.
- (92) Wiebe, R.; Gaddy, V. L.; Heins, C. Solubility of Hydrogen in Water at 250 °C from 25 to 1000 atm. *Ind. Eng. Chem.* **1932**, *24*, 823.
- (93) Rahbari, A.; Garcia-Navarro, J. C.; Ramdin, M.; van den Broeke, L. J. P.; Moultsos, O. A.; Dubbeldam, D.; Vlugt, T. J. H. Effect of water content on thermodynamic properties of compressed hydrogen. *J. Chem. Eng. Data* **2021**, *66*, 2071–2087.
- (94) Lopez-Lazaro, C.; Bachaud, P.; Moretti, I.; Ferrando, N. Predicting the phase behavior of hydrogen in NaCl brines by molecular simulation for geological applications. *Bulletin de la Société Géologique de France* **2019**, *190*, 7.
- (95) van Rooijen, W. A.; Habibi, P.; Xu, K.; Dey, P.; Vlugt, T. J. H.; Hajibeygi, H.; Moultsos, O. A. Interfacial Tensions, Solubilities, and Transport Properties of the $\text{H}_2/\text{H}_2\text{O}/\text{NaCl}$ System: A Molecular Simulation Study. *J. Chem. Eng. Data* **2024**, *69*, 307–319.
- (96) Shi, W.; Maginn, E. J. Continuous Fractional Component Monte Carlo: An Adaptive Biasing Method for Open System Atomistic Simulations. *J. Chem. Theory Comput.* **2007**, *3*, 1451–1463.
- (97) Shi, W.; Maginn, E. J. Improvement in Molecule Exchange Efficiency in Gibbs Ensemble Monte Carlo: Development and Implementation of the Continuous Fractional Component Move. *J. Comput. Chem.* **2008**, *29*, 2520–2530.
- (98) Hens, R.; Rahbari, A.; Caro-Ortiz, S.; Dawass, N.; Erdős, M.; Pouraeidesfahani, A.; Salehi, H. S.; Celebi, A. T.; Ramdin, M.; Moultsos, O. A.; Dubbeldam, D.; Vlugt, T. J. H. Brick-CFCMC: Open source software for Monte Carlo simulations of phase and reaction equilibria using the Continuous Fractional Component method. *J. Chem. Inf. Model.* **2020**, *60*, 2678–2682.
- (99) Rahbari, A.; Hens, R.; Ramdin, M.; Moultsos, O. A.; Dubbeldam, D.; Vlugt, T. J. H. Recent advances in the continuous fractional component Monte Carlo methodology. *Mol. Sim.* **2021**, *47*, 804–823.
- (100) Polat, H. M.; Salehi, H. S.; Hens, R.; Wasik, D. O.; Rahbari, A.; De Meyer, F.; Houriez, C.; Coquelet, C.; Calero, S.; Dubbeldam, D.; Moultsos, O. A.; Vlugt, T. J. H. New features of the open source Monte Carlo software Brick-CFCMC: Thermodynamic integration and hybrid trial moves. *J. Chem. Inf. Model.* **2021**, *61*, 3752–3757.
- (101) Köster, A.; Thol, M.; Vrabec, J. Molecular models for the Hydrogen age: Hydrogen, Nitrogen, Oxygen, Argon, and Water. *J. Chem. Eng. Data* **2018**, *63*, 305–320.
- (102) Marx, D.; Nielaba, P. Path-integral Monte Carlo techniques for rotational motion in two dimensions: Quenched, annealed, and no-spin quantum-statistical averages. *Phys. Rev. A* **1992**, *45*, 8968–8971.
- (103) Tsimpanogiannis, I. N.; Maity, S.; Celebi, A. T.; Moultsos, O. A. Engineering Model for Predicting the Intradiffusion Coefficients of Hydrogen and Oxygen in Vapor, Liquid, and Supercritical Water based on Molecular Dynamics Simulations. *J. Chem. Eng. Data* **2021**, *66*, 3226–3244.
- (104) Sesé, L. M. Study of the Feynman-Hibbs effective potential against the path-integral formalism for Monte Carlo simulations of quantum many-body Lennard-Jones systems. *Mol. Phys.* **1994**, *81*, 1297–1312.
- (105) Sesé, L. M. Feynman-Hibbs potentials and path integrals for quantum Lennard-Jones systems: Theory and Monte Carlo simulations. *Mol. Phys.* **1995**, *85*, 931–947.
- (106) Zeron, I. M.; Abascal, J. L. F.; Vega, C. A force field of Li^+ , Na^+ , K^+ , Mg^{2+} , Ca^{2+} , Cl^- , and SO_4^{2-} in aqueous solution based on the TIP4P/2005 water model and scaled charges for the ions. *J. Chem. Phys.* **2019**, *151*, 134504.

- (107) Thompson, A. P.; Aktulgah, H. M.; Berger, R.; Bolintineanu, D. S.; Brown, W. M.; Crozier, P. S.; in 't Veld, P. J.; Kohlmeyer, A.; Moore, S. G.; Nguyen, T. D.; Shan, R.; Stevens, M. J.; Tranchida, J.; Trott, C.; Plimpton, S. J. LAMMPS - a flexible simulation tool for particle-based materials modeling at the atomic, meso, and continuum scales. *Comput. Phys. Commun.* **2022**, *271*, 108171.
- (108) Lemmon, E. W.; Bell, I. H.; Huber, M. L.; McLinden, M. O. *NIST Standard Reference Database 23: Reference Fluid Thermodynamic and Transport Properties-REFPROP*, version 10.0; National Institute of Standards and Technology, 2018. <https://www.nist.gov/srd/refprop>.
- (109) Bird, R. B.; Stewart, W. E.; Lightfoot, E. N. *Transport Phenomena*, 2nd ed.; John Wiley & Sons: New York, 2007.
- (110) Treybal, R. E. *Mass-Transfer Operations*, 3rd ed.; McGraw-Hill Book Company: Singapore, 1980.
- (111) Jamali, S. H.; Wolff, L.; Becker, T. M.; De Groen, M.; Ramdin, M.; Hartkamp, R.; Bardow, A.; Vlugt, T. J. H.; Moults, O. A. OCTP: A tool for on-the-fly calculation of transport properties of fluids with the order-n algorithm in LAMMPS. *J. Chem. Inf. Model.* **2019**, *59*, 1290–1294.
- (112) Taylor, R.; Kooijman, H. A. Composition derivatives of activity coefficient models (for the estimation of thermodynamic factors in diffusion). *Chem. Eng. Commun.* **1991**, *102*, 87–106.
- (113) Keffer, D. J.; Gao, C. Y.; Edwards, B. J. On the relationship between Fickian diffusivities at the continuum and molecular levels. *J. Phys. Chem. B* **2005**, *109*, 5279–5288.
- (114) Hulikal Chakrapani, T.; Hajibeygi, H.; Moults, O. A.; Vlugt, T. J. H. Calculating Thermodynamic Factors for Diffusion Using the Continuous Fractional Component Monte Carlo Method. *J. Chem. Theory Comput.* **2024**, *20*, 333–347.
- (115) Poursaeidesfahani, A.; Torres-Knoop, A.; Dubbeldam, D.; Vlugt, T. J. H. Direct free energy calculation in the Continuous Fractional Component Gibbs ensemble. *J. Chem. Theory Comput.* **2016**, *12*, 1481–1490.
- (116) Jamali, S. H.; Wolff, L.; Becker, T. M.; Bardow, A.; Vlugt, T. J. H.; Moults, O. A. Finite-Size Effects of Binary Mutual Diffusion Coefficients from Molecular Dynamics. *J. Chem. Theory Comput.* **2018**, *14*, 2667–2677.
- (117) Moults, O. A.; Tsipanogiannis, I. N.; Panagiotopoulos, A. Z.; Economou, I. G. Self-Diffusion Coefficients of the Binary ($\text{H}_2\text{O} + \text{CO}_2$) Mixture at High Temperatures and Pressures. *J. Chem. Thermodyn.* **2016**, *93*, 424–429.
- (118) Yeh, I. C.; Hummer, G. System-size dependence of diffusion coefficients and viscosities from molecular dynamics simulations with periodic boundary conditions. *J. Phys. Chem. B* **2004**, *108*, 15873–15879.
- (119) Celebi, A. T.; Dawass, N.; Moults, O. A.; Vlugt, T. J. H. How sensitive are physical properties of choline chloride–urea mixtures to composition changes: Molecular dynamics simulations and Kirkwood–Buff theory. *J. Chem. Phys.* **2021**, *154*, 184502.
- (120) Celebi, A. T.; Jamali, S. H.; Bardow, A.; Vlugt, T. J. H.; Moults, O. A. Finite-size effects of diffusion coefficients computed from molecular dynamics: a review of what we have learned so far. *Mol. Sim.* **2021**, *47*, 831–845.
- (121) Krishna, R.; van Baten, J. M. The Darken Relation for Multicomponent Diffusion in Liquid Mixtures of Linear Alkanes: An Investigation Using Molecular Dynamics (MD) Simulations. *Ind. Eng. Chem. Res.* **2005**, *44*, 6939–6947.
- (122) Wolff, L.; Jamali, S. H.; Becker, T. M.; Moults, O. A.; Vlugt, T. J. H.; Bardow, A. Prediction of Composition-Dependent Self-Diffusion Coefficients in Binary Liquid Mixtures: The Missing Link for Darken-Based Models. *Ind. Eng. Chem. Res.* **2018**, *57*, 14784–14794.
- (123) Polat, H. M.; de Meyer, F.; Houriez, C.; Moults, O. A.; Vlugt, T. J. H. Solving chemical absorption equilibria using free energy and quantum chemistry calculations: methodology, limitations, and new open-source software. *J. Chem. Theory Comput.* **2023**, *19*, 2616–2629.
- (124) Wells, B. A.; Chaffee, A. L. Ewald Summation for Molecular Simulations. *J. Chem. Theory Comput.* **2015**, *11*, 3684–3695.
- (125) Span, R.; Wagner, W. A new equation of state for carbon dioxide covering the fluid region from the triple-point temperature to 1100 K at pressures up to 800 MPa. *J. Phys. Chem. Ref. Data* **1996**, *25*, 1509–1596.
- (126) Moults, O. A.; Zhang, Y.; Tsipanogiannis, I. N.; Economou, I. G.; Maginn, E. J. System-Size Corrections for the Self-Diffusion Coefficients Calculated from Molecular Dynamics Simulations: The Case of CO_2 , n-Alkanes, and poly(ethylene glycol) dimenthyl ethers. *J. Chem. Phys.* **2016**, *145*, 074109.
- (127) Barrat, J.-L.; Hansen, J.-P. *Basic Concepts for Simple and Complex Liquids*, 1st ed.; Cambridge University Press: Cambridge, 2003.
- (128) Van Loef, J. J. Temperature and density dependence of the self-diffusion coefficient in simple liquids. *Physica* **1972**, *62*, 345–356.
- (129) Harris, K. R.; Trappeniers, N. J. The density dependence of the self-diffusion coefficient of liquid methane. *Phys. A (Amsterdam, Neth.)* **1980**, *104*, 262–280.
- (130) Clark, W. M.; Rowley, R. L. The mutual diffusion coefficient of methanol–n-hexane near the consolute point. *AIChE J.* **1986**, *32*, 1125–1131.
- (131) Wu, G.; Fiebig, M.; Leipertz, A. Messung des binären Diffusionskoeffizienten in einem Entmischungssystem mit Hilfe der Photonen-Korrelationsspektroskopie. *Waerme- Stoffuebertrag.* **1988**, *22*, 365–371.
- (132) De, S.; Shapir, Y.; Chimowitz, E. H. Scaling of self and Fickian diffusion coefficients in the critical region. *Chem. Eng. Sci.* **2001**, *56*, 5003–5010.
- (133) Matos Lopes, M. L. S.; Nieto de Castro, C. A.; Sengers, J. V. Mutual diffusivity of a mixture of n-hexane and nitrobenzene near its consolute point. *Int. J. Thermophys.* **1992**, *13*, 283–294.
- (134) Moggridge, G. D. Prediction of the mutual diffusivity in binary liquid mixtures containing one dimerising species, from the tracer diffusion coefficients. *Chem. Eng. Sci.* **2012**, *76*, 199–205.
- (135) Gavril, D.; Atta, K. R.; Karaiskakis, G. Determination of collision cross-sectional parameters from experimentally measured gas diffusion coefficients. *Fluid Phase Equilib.* **2004**, *218*, 177–188.
- (136) Saxena, S. C.; Mason, E. A. Thermal diffusion and the approach to the steady state in gases: II. *Mol. Phys.* **1959**, *2*, 379–396.
- (137) Weissman, S. Estimation of Diffusion Coefficients from Viscosity Measurements: Polar and Polyatomic Gases. *J. Chem. Phys.* **1964**, *40*, 3397–3406.
- (138) Tödheide, K.; Franck, E. U. Das Zweiphasengebiet und die kritische Kurve im System Kohlendioxid–Wasser bis zu Drucken von 3500 bar. *Z. Phys.* **1963**, *37*, 387–401.
- (139) Hyde, A. M.; Zultanski, S. L.; Waldman, J. H.; Zhong, Y.-L.; Shevlin, M.; Peng, F. General Principles and Strategies for Salting-Out Informed by the Hofmeister Series. *Org. Process Res. Dev.* **2017**, *21*, 1355–1370.
- (140) Setschenow, J. Über die konstitution der salzlösungen aufgrund ihres verhaltens zu kohlensäure. *Z. Phys. Chem.* **1889**, *4*, 117–125.
- (141) Loschmidt, J. J. Experimental-Untersuchungen über die Diffusion von Gasen ohne poröse Scheidewände I. *Sitzungsber. Kais. Akad. Wiss. Wien* **1870**, *61*, 367–380.
- (142) Loschmidt, J. J. Experimental-Untersuchungen über die Diffusion von Gasen ohne poröse Scheidewände II. *Sitzungsber. Kais. Akad. Wiss. Wien* **1870**, *62*, 468–478.
- (143) Schmidt, R. Diss. Halle 1904. *Ann.d. Phys.* **1904**, *14* (4), 801.
- (144) Lonius, A. Die abhängigkeit des gasdiffusionskoeffizienten vom mischungsverhältnis. *Ann. Phys.* **1909**, *334*, 664–678.
- (145) Boardman, L. E.; Wild, N. E. The diffusion of pairs of gases with molecules of equal mass. *Proc. R. Soc. A* **1937**, *162*, 511–520.
- (146) Suetin, P. E.; Shchegolev, G. T.; Klestov, R. A. *Soviet Phys.-Technol. Phys.* **1960**, *4*, 964.
- (147) Suetin, P. E.; Ivakin, B. A. Coefficients of mutual diffusion of some gases measured by optical method (English Translation). *Soviet Phys.-Technol. Phys.* **1961**, *1*, 359–361.
- (148) Ivakin, B. A.; Suetin, P. E. *Soviet Phys.-Technol. Phys.* **1964**, *9*, 866.

- (149) von Obermayer, A. Ueber die Abhangigkeit des Diffusionskoeffizienten der Gase von der Temperatur. *Sitzungsber. Kais. Akad. Wiss. Wien* **1880**, *81*, 1102.
- (150) von Obermayer, A. Versuche uber die Diffusion von Gasen. *Sitzungsber. Kais. Akad. Wiss. Wien* **1882**, *85*, 147.
- (151) von Obermayer, A. Versuche uber Diffusion III. *Sitzungsber. Kais. Akad. Wiss. Wien* **1883**, *87*, 188.
- (152) Schafer, K.; Corte, H.; Moesta, H. Uber die Messung der Temperatur-und Konzentrations-Abhangigkeit des Diffusionskoeffizienten von Gasen. *Zeitschrift fur Elektrochemie und angewandte physikalische Chemie* **1951**, *55*, 662–664.
- (153) Lonsdale, H. K.; Mason, E. A. Thermal Diffusion and the Approach to the Steady State in H₂–CO₂ and He–CO₂. *J. Phys. Chem.* **1957**, *61*, 1544–1551.
- (154) Bondarenko, A. G.; Golubev, I. F. *Gasov. Prom* **1964**, *9*, 50.
- (155) Miller, L.; Carman, P. C. Self-diffusion in mixtures. Part 6.—Self-diffusion of hydrogen in certain gaseous mixtures. *Trans. Faraday Soc.* **1964**, *60*, 33–37.
- (156) Annis, B. K.; Humphreys, A. E.; Mason, E. A. Nonisothermal, Nonstationary Diffusion. *Phys. Fluids* **1969**, *12*, 78–83.
- (157) Miller, L.; Carman, P. C. Self-diffusion in mixtures. Part 4.—Comparison of theory and experiment for certain gas mixtures. *Trans. of the Faraday Soc.* **1961**, *57*, 2143–2150.
- (158) Waldmann, L. Die Temperaturscheinungen bei der Diffusion. *Naturwiss* **1944**, *32*, 222–223.
- (159) Waldmann, L. Die Temperaturscheinungen bei der Diffusion in ruhenden Gasen und ihre metechnische Anwendung. *Z. Phys.* **1947**, *124*, 2–29.
- (160) Mason, E. A.; Miller, L.; Spurling, T. H. Pressure Dependence of the Diffusion Thermoeffect in Gases (Dufour Effect). *J. Chem. Phys.* **1967**, *47*, 1669–1675.
- (161) Kestin, J.; Ro, S.; Wakeham, W. A. The transport properties of binary mixtures of hydrogen with CO, CO₂ and CH₄. *Phys. A (Amsterdam, Neth.)* **1983**, *119*, 615–638.
- (162) Wicke, E.; Hugo, P. Gleitungserscheinungen bei der Gasdiffusion. *Z. Phys. Chem.* **1961**, *28*, 401–421.
- (163) Schneider, M.; Schafer, K. Gasdiffusionsmessungen zwischen 273 und 1300 °K. *Ber. der Bunsenges. Phys. Chem.* **1969**, *73*, 702–706.
- (164) Kosov, N. D.; Zhalgasov, A. *Soviet Phys.-Technol. Phys.* **1970**, *40*, 1325.
- (165) Giddings, J. C.; Seager, S. L. Method for the Rapid Determination of Diffusion Coefficients. Theory and Application. *Ind. Eng. Chem. Fundamen.* **1962**, *1*, 277–283.
- (166) Vyshenskaya, V. F.; Kosov, N. D. Issledovanie Protsessov Perenosu. *Voprosy Teorii Otnositel'nosti Alma Ata. Sbornik.* **1959**, *61*, 114–125.
- (167) McCarty, K. P.; Mason, E. A. Kirkendall effect in gaseous diffusion. *Phys. Fluids* **1960**, *3*, 908–922.
- (168) Boyd, C. A.; Stein, N.; Steingrimsson, V.; Rumpel, W. F. An Interferometric Method of Determining Diffusion Coefficients in Gaseous Systems. *J. Chem. Phys.* **1951**, *19*, 548–553.
- (169) Wiebe, R.; Gaddy, V. L. The Solubility in Water of Carbon Dioxide at 50, 75 and 100°, at Pressures to 700 Atmospheres. *J. Am. Chem. Soc.* **1939**, *61*, 315–318.
- (170) Takenouchi, S.; Kennedy, G. C. The binary system H₂O-CO₂ at high temperatures and pressures. *Am. J. Sci.* **1964**, *262*, 1055–1074.
- (171) Takenouchi, S.; Kennedy, G. C. The solubility of carbon dioxide in NaCl solutions at high temperatures and pressures. *Am. J. Sci.* **1965**, *263*, 445–454.
- (172) Kling, G.; Maurer, G. The solubility of hydrogen in water and in 2-aminoethanol at temperatures between 323 K and 423 K and pressures up to 16 MPa. *J. Chem. Thermodyn.* **1991**, *23*, 531–541.
- (173) Wiebe, R.; Gaddy, V. L. The Solubility of Hydrogen in Water at 0, 50, 75 and 100° from 25 to 1000 Atmospheres. *J. Am. Chem. Soc.* **1934**, *56*, 76–79.